

Genetic screen for suppression of transcriptional interference reveals fission yeast 14–3–3 protein Rad24 as an antagonist of precocious Pol2 transcription termination

Angad Garg¹, Stewart Shuman^{1,*} and Beate Schwer^{2,*}

¹Molecular Biology Program, Memorial Sloan Kettering Cancer Center, New York, NY 10065, USA and ²Dept. of Microbiology and Immunology, Weill Cornell Medical College, New York, NY 10065, USA

Received July 12, 2021; Revised December 01, 2021; Editorial Decision December 06, 2021; Accepted December 13, 2021

ABSTRACT

Expression of fission yeast Pho1 acid phosphatase is repressed under phosphate-replete conditions by transcription of an upstream *prt* lncRNA that interferes with the *pho1* mRNA promoter. lncRNA control of *pho1* mRNA synthesis is influenced by inositol pyrophosphate (IPP) kinase Asp1, deletion of which results in *pho1* hyper-repression. A forward genetic screen for ADS (Asp1 Deletion Suppressor) mutations identified the 14–3–3 protein Rad24 as a governor of phosphate homeostasis. Production of full-length interfering *prt* lncRNA was squelched in *rad24Δ* cells, concomitant with increased production of *pho1* mRNA and increased Pho1 activity, while shorter precociously terminated non-interfering *prt* transcripts persisted. Epistasis analysis showed that *pho1* de-repression by *rad24Δ* depends on: (i) 3'-processing and transcription termination factors CPF, Pin1, and Rhn1; and (ii) Threonine-4 of the Pol2 CTD. Combining *rad24Δ* with the IPP pyrophosphatase-dead *asp1-H397A* allele caused a severe synthetic growth defect that was ameliorated by loss-of-function mutations in CPF, Pin1, and Rhn1, and by CTD phospho-site mutations T4A and Y1F. Rad24 function in repressing *pho1* was effaced by mutation of its phosphate-binding pocket. Our findings instate a new role for a 14–3–3 protein as an antagonist of precocious RNA 3'-processing/termination.

INTRODUCTION

Inorganic phosphate is an essential nutrient. Cells from all domains of life respond to acute phosphate limita-

tion by inducing the transcription of phosphate acquisition genes encoding secreted or cell-surface associated enzymes that mobilize phosphate from the extracellular environment and transmembrane transporters of inorganic phosphate or simple phosphate-containing compounds. The fission yeast phosphate homeostasis (*PHO*) genes *pho1* (acid phosphatase), *pho84* (phosphate transporter), and *tgp1* (glycerophosphate transporter) are repressed in phosphate-rich medium by transcription of upstream lncRNAs—*prt*, *prt2* and *nc-tgp1*, respectively (1). lncRNA synthesis interferes with *PHO* mRNA synthesis by displacing the activating transcription factor Pho7 from its binding site(s) in the mRNA promoters (2–4). lncRNA control of the *PHO* genes is influenced by the Ser7 and Ser5 phospho-sites in the RNA polymerase II CTD, the protein kinases Csk1 and Cdk9, and the inositol pyrophosphate (IPP) pyrophosphatases Asp1 and Aps1, mutations of which lead to precocious 3'-polyadenylation and termination of lncRNA transcription prior to the mRNA promoter, thereby alleviating the transcriptional interference and de-repressing the *PHO* genes in phosphate-replete cells (5–12). A mutation in the Pol2 Rpb1 subunit that slows elongation rate de-represses the *PHO* genes, likely by prolonging the kinetic window for precocious lncRNA 3'-processing/termination (13). The *PHO* regulon is also de-repressed by a gain-of-function mutation in the essential Pol2 termination factor Seb1 (14). By contrast, mutations of the Thr4 phospho-site in the RNA polymerase II CTD, the 3'-cleavage and polyadenylation factor CPF, the transcription termination factor Rhn1, and the inositol pyrophosphate kinase Asp1 result in hyper-repression of *PHO* gene expression—by antagonizing precocious 3'-processing/termination of lncRNA transcription and thereby increasing transcriptional interference at the mRNA promoter (6,7,10,11).

De-repression of the three *PHO* genes is the hallmark of the fission yeast transcriptional response to acute phosphate starvation (2). The parsimonious model is that phos-

*To whom correspondence should be addressed. Tel: +1 212 639 7145; Email: s-shuman@ski.mskcc.org
Correspondence may also be addressed to Beate Schwer. Tel: +1 212 746 6518; Email: bschwer@med.cornell.edu

phate deprivation triggers a signaling pathway that ultimately results in shut-off of transcription of the *pri*, *pri2*, and *nc-tgp1* lncRNAs. Yet, the mechanism of phosphate sensing in fission yeast is obscure and it is not known how a starvation signal is transmitted to impact lncRNA transcription initiation by Pol2. Indeed, the transcription factor(s) that drive the lncRNA promoters remain to be identified.

In an effort to better understand how the *CTD-T4A* mutation affects interference, and to potentially identify agents of *pri* lncRNA transcription, we performed a forward genetic screen in *CTD-T4A* cells for extragenic suppressors of the *pho1* hyper-repressive phenotype (12). We envisioned two possible classes of *STF* (Suppressor of Threonine Four) mutations: (i) those that reduce or shut off transcription of the *pri* lncRNA and thereby relieve *pri* interference with the *pho1* promoter; and (ii) those that enhance the 3'-processing/termination efficiency of the T4A mutant Pol2 transcription complex engaged in *pri* lncRNA synthesis. Analysis of 18 independent *STF* isolates revealed, in every case, a mutation in the C-terminal pyrophosphatase domain of Asp1 (12), a bifunctional inositol pyrophosphate (IPP) kinase/pyrophosphatase that interconverts 5-IP7 and 1,5-IP8 (15,16). Focused characterization of two *STF* strains identified 51 coding genes coordinately up-regulated *vis-à-vis* the parental *T4A* strain, including all three *PHO* regulon genes. Whereas these two *STF* alleles—*asp1-386* (*Stop*) and *asp1-493* (*Stop*)—were lethal in a wild-type CTD background, they were viable in combination with mutations in CPF and Rhn1, in which context Pho1 was also depressed (12). These findings implicated the Asp1 pyrophosphatase in constraining 1,5-IP8 (or 1-IP7) synthesis by Asp1 kinase, without which 1-IPPs can accumulate to toxic levels that elicit precocious termination by CPF/Rhn1.

Whereas the results of the *STF* screen fortify the case for IPPs IP8 and/or 1-IP7 as agonists of 3'-processing/termination, they do not shed light on non-IPP modulators of lncRNA-dependent transcriptional interference with the *PHO* regulon, including those that drive the lncRNA promoter. To circumvent the issue of IPP dynamics, we sought to implement a different genetic screen for mutations that overcome the hyper-repression of acid phosphatase activity in phosphate-replete *asp1*Δ cells, which are unable to synthesize 1,5-IP8 or 1-IP7 (15,16).

We describe here the isolation and characterization of five independent *ADS* (*Asp1* *Deletion* *Suppressor*) mutants affecting four fission yeast genes: *rad24*, *csk1*, *tnr3*, and *SPBP8B7.17c*. *Tnr3* and *SPBP8B7.17c* are essential enzymes involved in the synthesis of thiamine pyrophosphate. *ADS* mutations in these two genes up-regulated the expression of two paralogous acid phosphatase enzymes: the thiamine-repressible acid phosphatase Pho4 and the phosphate-repressible Pho1. By contrast, *ADS* mutations in *rad24* (a 14–3–3 protein) and *csk1* (a CDK-activating protein kinase) exclusively de-repressed Pho1 expression under phosphate-replete conditions, as did *rad24*Δ and *csk1*Δ null mutations. We provide genetic, transcriptomic, and biochemical evidence that absence of Rad24 de-represses the *PHO* regulon by promoting precocious termination of interfering lncRNA transcription.

MATERIALS AND METHODS

Mutagenesis of *asp1*Δ cells and screening for increased acid phosphatase expression

Ethyl methanesulfonate (EMS) mutagenesis was carried out as described (17). In brief, *asp1*Δ cells were grown in minimal medium (PMG) at 30°C to an A_{600} of 0.25. Cells were harvested by centrifugation and resuspended at $\sim 1 \times 10^8$ cells/ml in PMG medium. To one aliquot (2 ml), we added EMS (Sigma) to a final concentration of 2%, while a second aliquot was left untreated (to determine survival rate). The suspensions were placed on a nutator and incubated for 3.5 h at room temperature. Cells were washed thrice with NaCl (150 mM), diluted, and plated to YES agar. After 6 days of incubation at 30°C, plates were overlaid with 1% agarose containing 0.015% α -naphthyl phosphate, 0.15% Fast Blue B Salt stain, and 0.1 M sodium acetate (pH 4.2) to assay acid phosphatase activity. Colonies that turned red were extracted from near confluent lawns of mutagenized cells and colony-purified by streaking or re-plating at low cell densities. Independently isolated candidate suppressor strains were back-crossed to *asp1*Δ cells of the opposite mating type, subjected to random spore analysis, and identified as red colonies using the overlay assay. After back-crossing individual suppressor strains for a second time, we measured acid phosphatase activity of cells grown in liquid culture (YES medium) at 30°C, as follows. Exponentially growing cultures were harvested, washed, and resuspended in water. Reaction mixtures (200 μ l) containing 10 mM *p*-nitrophenylphosphate, 100 mM sodium acetate (pH 4.2), and serial dilutions of cells were incubated at 30°C for 5 min. To stop the reaction, 1 ml of 1 M sodium carbonate was added, the cells were removed by centrifugation, and the absorbance of the supernatant at 410 nm was measured. Acid phosphatase activity is expressed as the ratio of A_{410} (*p*-nitrophenol production) to A_{600} (cells). The data are averages (\pm SEM) of measurements from at least three independent cultures.

Spot tests of fission yeast growth

Cultures of *Schizosaccharomyces pombe* strains were grown in liquid YES (yeast extract with supplement) medium until A_{600} reached 0.5–0.8. The cultures were adjusted to an A_{600} of 0.1 and aliquots (3 μ l) of serial 5-fold dilutions were spotted to YES agar. The plates were photographed after incubation for 2 days at 34°C, 2.5 days at 30°C and 37°C, 4 days at 25°C, and 6 days at 20°C.

Whole-genome sequencing

After PicoGreen quantification and quality control by Agilent BioAnalyzer, 500 ng aliquots of genomic DNA were sheared using a LE220-plus Focused-ultrasonicator (Covaris catalog #500569) and sequencing libraries were prepared using the KAPA Hyper Prep Kit (Kapa Biosystems KK8504) with modifications. DNA libraries were subjected to size selection by mixture with 0.5 vol of AMPure XP beads (Beckman Coulter catalog #A63882) after post-ligation cleanup. Libraries were not amplified by PCR and were pooled equivolume for sequencing. Samples were run

on a NovaSeq 6000 in a 150 bp/150 bp paired-end run using the NovaSeq 6000 SBS v1 Kit and an S1 flow cell (Illumina). The average number of read pairs per sample was 10 million.

Mapping suppressor mutations

The FASTA file for the *S. pombe* genome was accessed from Pombase. The whole-genome sequencing data from the parental and suppressor mutant strains were aligned to the genome using Bowtie2 (18). The resulting SAM files were converted to BAM files using Samtools (19). Variants were identified by BCFtools (20) using the criteria of adjusted mapping quality = 40, minimum base quality = 20, and disabled probabilistic realignment for the computation of base alignment quality (BAQ) for considering variations or insertion-deletion events. The multi-allelic caller protocol was used for variant calling in BCFtools. Variants were annotated using SnpEff, with its in-built genome version for *S. pombe* (21). Variants were further filtered by removing all variations with an average mapping quality ≤ 25 (Phred scale). All variants present in the parental strain were excluded as non-causal mutations.

Northern blot analyses

Total RNA was extracted via the hot phenol method (22) from six A_{600} units of yeast cells that had been grown exponentially in YES + G418 (for selection of *kanMX* plasmids) to A_{600} of 0.3 to 0.5 at 30°C. Aliquots (10 μ g) of total RNA were resolved by electrophoresis through a 1.2% agarose/formaldehyde gel. After photography under UV light to visualize ethidium bromide-stained rRNAs and tRNAs, the gel contents were transferred to a Hybond-XL membrane (GE Healthcare). Hybridization was performed with a 5' 32 P-labeled ssDNA complementary to nucleotides 160–202 or 84–115 downstream of the *prt* or *pho1* transcription start sites, respectively, using a commercial hybridization buffer (Invitrogen ULTRAhyb-Oligo). Hybridized probes were visualized by autoradiography and quantified in ImageQuant after scanning the blot with a phosphorimager.

Deletion of *rad24*⁺ and allelic exchange at the *rad24* locus

rad24 DNA segments [–585 to –1 and +1217 to +1541 relative to the +1 nucleotide of the *rad24* translational start codon], were PCR amplified and cloned upstream and downstream, respectively, of the *natMX* antibiotic resistance gene in a bacterial plasmid. The *rad24* Δ ::*natMX* gene disruption cassette was excised from the plasmid and transfected into diploid *S. pombe* cells. Nourseothricin-resistant transformants were selected and analyzed by Southern blotting to confirm correct integration at one of the *rad24* loci. Heterozygous diploids were sporulated and nourseothricin-resistant *rad24* Δ haploids were isolated. Hygromycin or geneticin-resistant *rad24* Δ strains were generated by marker switching (23).

The *rad24* allelic exchange integration cassettes were generated in a bacterial plasmid by standard cloning procedures. The *rad24* ORF was PCR-amplified from *S. pombe*

cDNA with oligonucleotide primers that introduced restriction sites for cloning. Two-stage PCR overlap extension with mutagenic primers was used to introduce missense mutations into the *rad24* ORF. The integration cassettes consisted of the following elements, proceeding from 5' to 3': (i) a 585-bp segment of genomic DNA 5' of the *rad24*⁺ start codon; (ii) an intron-less ORF encoding wild-type or mutant Rad24, with or without an in-frame C-terminal tandem affinity purification (TAP) tag; (iii) a 258-bp segment of genomic DNA 3' of the *nmt1*⁺ stop codon containing polyA/termination signals from the *nmt1*⁺ gene; (iv) a *kanMX* gene conferring resistance to G418 and (v) a 323-bp segment of genomic DNA 3' of the *rad24*⁺ stop codon. The integration cassettes were excised from the plasmids and transfected into a diploid strain. G418-resistant diploids were selected and a segment of the *rad24*::*kanMX* allele was PCR amplified and sequenced to verify that the desired alleles were present. Correct integrations at the target locus were verified by Southern blotting. Confirmed heterozygous diploids were sporulated and G418-resistant haploid progeny were selected. Strain genotypes are provided in Supplementary Table S1.

Double and triple mutants

Standard genetic methods were employed to generate haploid strains harboring mutations/deletions in two (or three) differently marked genes. In brief, pairs of haploids with null or missense mutations were mixed on malt agar to allow mating and sporulation; the mixture was then subjected to random spore analysis. Spores (~1500) were plated on YES agar and also on media selective for marked mutant alleles; the plates were incubated at 30°C for up to 5 days to allow slow growing progeny to germinate and form colonies. At least 500 viable progeny were screened by replica plating for the presence of the second (and then third) marker gene, or by sequentially replica-plating from YES to selective media. Strain genotypes are provided in Supplementary Table S1.

Transcriptome profiling by RNA-seq

RNA was isolated from *S. pombe rad24* Δ cells and wild-type control cells that were grown in liquid YES medium at 30°C to an A_{600} of 0.5–0.6. Cells were harvested by centrifugation and total RNA was extracted via the hot phenol method. The integrity of total RNA was gauged with an Agilent Technologies 2100 Bioanalyzer. The Illumina TruSeq stranded mRNA sample preparation kit was used to purify poly(A)⁺ RNA from 500 ng of total RNA and to carry out the subsequent steps of poly(A)⁺ RNA fragmentation, strand-specific cDNA synthesis, indexing, and amplification. Indexed libraries were normalized and pooled for paired-end sequencing performed by using an Illumina NovaSeq 6000-S1 flow cell. FASTQ files bearing paired-end reads (51 bases in length) were mapped to the *S. pombe* genome (Pombase) using HISAT2-2.1.0 with default parameters (24). The resulting SAM files were converted to BAM files using Samtools. Count files for individual replicates were generated with HTSeq-0.10.0 (25) using exon annotations from Pombase (GFF annotations, genome-version ASM294v2; source 'ensembl'). RPKM analysis and

pairwise correlations were performed as described previously (6). Differential gene expression and fold change analysis was performed in DESeq2 (26). Cut-off for further evaluation was set for genes that had an adjusted *P*-value (Benjamini-Hochberg corrected) of ≤ 0.05 and were up or down by at least two-fold in *rad24* Δ in comparison to wild-type. Genes were further filtered on the following criteria: (i) ≥ 2 -fold up and the average normalized read count for the mutant strain was ≥ 100 ; and (ii) ≥ 2 -fold down and the average normalized read count for the wild-type strain was ≥ 100 .

RESULTS

The *ADS* screen

asp1 Δ cells were mutagenized by treatment with 2% ethyl methanesulfonate (EMS) for 3.5 h at 22°C to achieve a survival rate of $\sim 30\%$. The cells were washed, plated on phosphate-replete YES agar medium, and incubated for 6 days at 30°C to allow formation of single colonies from individual mutagenized cells. To gauge acid phosphatase activity, the plates were overlaid with 1% agarose containing 0.015% α -naphthyl phosphate (a Pho1 substrate), 0.15% Fast Blue B Salt stain, and 0.1 M sodium acetate (pH 4.2). Cell surface acid phosphatase causes formation of a red pigment and relative red color intensity of the colonies provides a semi-quantitative assay of acid phosphatase activity (5,6,27). *asp1* Δ cells appear pale after this procedure. From an initial pool of about 280,000 EMS survivors, we picked 23 independent red colonies that we deemed candidate *ADS* mutants. These were re-streaked for single colonies, then grown out in YES liquid medium, replated, and re-tested for red color. The strains were then back-crossed to an *asp1* Δ strain of the opposite mating type and populations of post-sporulation haploid progeny were tested for acid phosphatase activity via the overlay assay. If the *ADS* phenotype resulted from a mutation in a single gene, then we expect $\sim 50\%$ of the haploid progeny from the back-cross to stain red and $\sim 50\%$ to be pale. We selected five of the back-crossed putative single-gene *ADS* mutants and back-crossed them for a second time to the original parental *asp1* Δ strain. 1:1 segregation of red/pale colony color was affirmed. Spot tests of the growth of the five independent twice back-crossed *ADS* strains and the *asp1* Δ parent on YES agar at 25 to 37°C is shown in Figure 1A. The *ADS* strains and the *asp1* Δ strain were assayed quantitatively for acid phosphatase activity after growth at 30°C in phosphate-replete liquid medium. The *ADS-1*, *ADS-2*, *ADS-3*, *ADS-4*, and *ADS-5* strains expressed 5-fold, 7-fold, 8-fold, 5-fold, and 12-fold higher acid phosphatase activity, respectively, than the *asp1* Δ parent (Figure 1B).

Fission yeasts elaborate two different cell-surface acid phosphatase enzymes: Pho1 and Pho4, both of which belong to the histidine acid phosphatase enzyme family. Pho1 expression is repressed under phosphate-replete and adenine-replete conditions and is de-repressed upon phosphate or adenine starvation (2,28–31). Pho4 expression is repressed under thiamine-replete conditions and is de-repressed by thiamine starvation (31–35). Thiamine status also affects Pho1 expression, i.e. *pho1* mRNA levels increase

in phosphate-replete cells that are starved for thiamine, albeit to a lesser extent than the increase elicited by phosphate starvation (30). Thus, the ensuing analysis of the output of the *ADS* screen focused on two issues: (i) mapping the mutations responsible for the *ADS* phenotype; and (ii) determining whether the *ADS* mutations that increase acid phosphatase activity do so via their effects on expression of Pho1, Pho4, or both.

Identification of *ADS* mutations by whole genome sequencing

Paired-end Illumina sequencing of unamplified genomic DNA (average read length 150 bases) from the parental *asp1* Δ strain and the five *ADS* strains was performed to achieve at least 100-fold coverage of each fission yeast genome. The mutations found in each of the five *ADS* strains are listed in Figure 1C. The *ADS*-associated lesions map to four genes with known or imputed roles in the repression of fission yeast acid phosphatase activity, either *per se* (in the case of *rad24* and *csk1*) or via their effects on thiamine metabolism (*tnr3* and *SPBP8B7.17c*).

tnr3 is an essential gene encoding a 569-aa enzyme required for synthesis of thiamine diphosphate (30). Tnr3 is a bifunctional enzyme composed of: (i) a C-terminal thiamine pyrophosphokinase domain, which transfers pyrophosphate from ATP to thiamine (36) and (ii) an N-terminal Nudix hydrolase domain that converts oxidized derivatives of thiamine diphosphate (oxothiamine and oxythiamine) to their respective monophosphates (37). *tnr3* (Thiamine Non-Repr^es^sible) was originally identified in a genetic screen for mutants that de-repress the expression of Pho4 acid phosphatase in cells grown in medium replete with thiamine (35). Subsequent studies showed that *tnr3* mutants also elicit a modest de-repression of Pho1 acid phosphatase in phosphate-replete cells (30). The *ADS-4* mutant isolated presently has a single missense mutation, Cys545Tyr, located in the C-terminal thiamine pyrophosphokinase domain (Figure 1C and Supplementary Figure S1C). The *ADS-5* strain has a different missense mutation, Asp460Asn, in the pyrophosphokinase domain. *ADS-5* also has a missense mutation in Not1, a subunit of the Ccr4-Not1 3'-deadenylase complex, and a splice-site mutation in the *tif452* gene encoding translation factor eIF4E (Figure 1C), neither of which is likely to cause the *ADS* phenotype. Reference to the crystal structure of the homodimeric mouse thiamine pyrophosphokinase in a product-like complex with pyrithiamine diphosphate, AMP, and magnesium (38) indicates that fission yeast Tnr3 amino acids Asp460 and Cys545 are constituents of the enzyme active site, which is composed of elements contributed by both subunits of the homodimer. The mouse and fission yeast thiamine pyrophosphokinases share 128 positions of amino acid side chain identity/similarity (Supplementary Figure S2). In particular, the motif RFDQ in the mouse enzyme (equivalent to ⁴⁵⁸RVDH⁴⁶¹ in Tnr3) directly engages the β phosphate of pyrithiamine diphosphate via hydrogen bonds from the arginine and glutamine side chains (Supplementary Figure S2). The intervening aspartate (Asp460 in Tnr3) makes a bidentate salt-bridge to the arginine that would be weakened or severed when it is replaced by asparagine (as in *ADS-5*). The downstream ²¹⁶STSN²¹⁹ motif

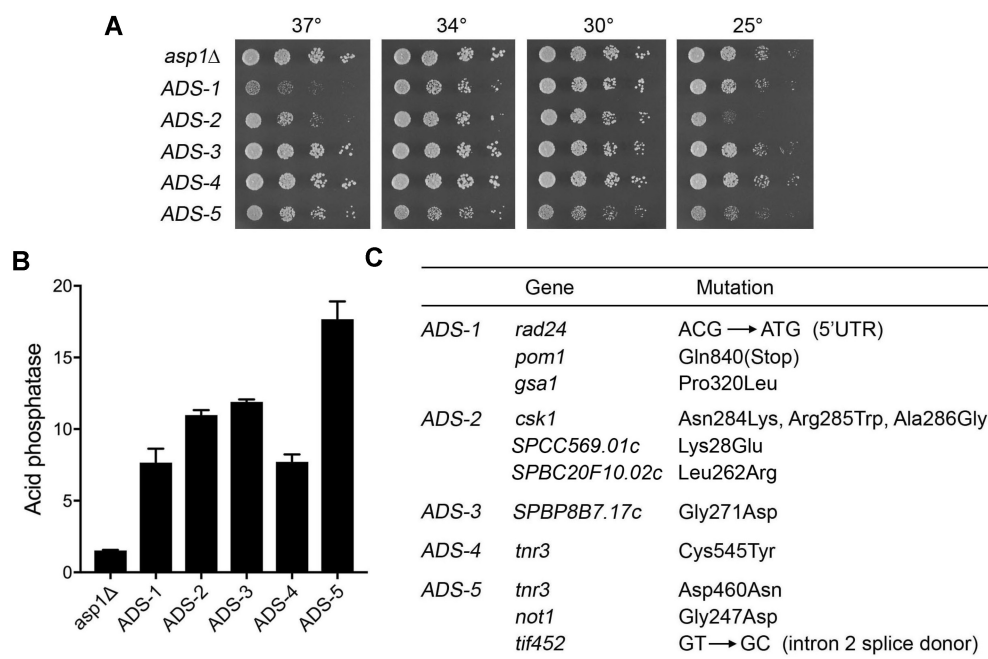


Figure 1. Fission yeast *ADS* mutants. (A) Serial 5-fold dilutions of *asp1Δ* and the indicated *ADS* strains were spotted on YES agar and grown at the indicated temperatures. (B) The *asp1Δ* and *ADS* strains were grown to A_{600} of 0.5 to 0.8 in liquid culture in YES medium at 30°C. Cells were then harvested, washed with water, and assayed for Pho1 acid phosphatase activity by conversion of *p*-nitrophenylphosphate to *p*-nitrophenol. Activity is expressed as the ratio of A_{410} (*p*-nitrophenol production) to A_{600} (input cells). (C) Whole-genome sequencing of twice back-crossed *ADS* strains revealed the indicated genetic mutations.

of the other subunit of the mouse homodimer (equivalent to $^{543}\text{SSCN}^{546}$ in Tnr3) contributes to the active site via a hydrogen bond from the Ser218 (Cys545 in Tnr3) to the β phosphate (Supplementary Figure S2). This contact would be perturbed by mutation to the bulkier Tyr side chain in the *ADS-4* strain.

SPBP8B7.17c is an essential gene encoding a 506-aa bifunctional enzyme involved in the salvage and biosynthesis pathways of thiamine metabolism. The N-terminal 271-aa of *SPBP8B7.17c* is the fission yeast homolog of the enzyme phosphomethylpyrimidine kinase (known as ThiD/J in bacteria) that sequentially converts 4-amino-5-hydroxymethyl-2-methylpyrimidine (HMP) to HMP-phosphate and then to HMP-pyrophosphate (39). A pairwise alignment of *SPBP8B7.17c* to *Escherichia coli* ThiJ (a 266-aa protein) highlights 125 positions of side chain identity/similarity (Supplementary Figure S3). The *ADS-3* mutant isolated presently has a single missense mutation, Gly271Asp (Figure 1C and Supplementary Figure S1D), located at the distal margin of the ThiD/J domain. This glycine is conserved in the *E. coli* ThiD enzyme (Supplementary Figure S3). The C-terminal domain of *SPBP8B7.17c* is homologous to thiaminase (known as TenA in bacteria), which catalyzes the hydrolysis of thiamine degradation products to regenerate HMP as part of the salvage pathway (40). The budding yeast ortholog of *SPBP8B7.17c* is Thi20 (551-aa; 211 positions of side chain identity/similarity), which has been characterized biochemically and structurally as a homodimeric enzyme with phosphomethylpyrimidine kinase and thiaminase activities (41,42). Thus, we propose that *SPBP8B7.17c/ADS-*

3 shall henceforth be referred to as fission yeast Thi20. The amino acids comprising the active site of the ThiD domain of budding yeast Thi20 (42) are all conserved in the fission yeast Thi20 protein, making it most likely that fission yeast Thi20 is a *bona fide* phosphomethylpyrimidine kinase. The parsimonious explanation for the isolation of mutants in essential thiamine pathway enzymes Tnr3 and Thi20 in the *ADS* screen is that these are hypomorphic alleles that reduce the intracellular levels of thiamine diphosphate (or some other thiamine metabolite) that acts as the signal for repression of one or both of the fission yeast acid phosphatase enzymes.

csk1 is an inessential gene that encodes a 306-aa cyclin-dependent kinase (Cdk)-activating protein kinase. Among its activities, Csk1 phosphorylates and activates Cdk9 (an essential protein kinase) and Cdk9, in turn, phosphorylates the Pol2 CTD and the CTD of elongation factor Spt5 (43). The *ADS-2* mutant isolated here has a triple missense mutation of three consecutive amino acids—Asn284Lys, Arg285Trp and Ala286Gly—located near the C-terminus of Csk1 (Figure 1C and Supplementary Figure S1B). Previous studies had shown that Pho1 acid phosphatase activity is de-repressed in a *csk1Δ* strain (2,5). This *csk1Δ* de-repression of Pho1 is erased by loss-of-function mutations of the Ssu72 phosphatase subunit of CPF and termination factor Rhn1 and is attenuated in the absence of CPF subunits Ctf1, Ppn1, and Swd22 (10). It is thought that Csk1 kinase activity is needed for *pvt* lncRNA-mediated interference with transcription from the downstream *pho1* mRNA promoter because it antagonizes precocious 3'-processing/termination during *pvt* lncRNA synthesis.

ADS-2 also has an incidental missense mutation in *SPCC569.01c* (encoding an inessential 323-aa protein of unknown function) and a missense mutation in *SPBC20F10.02c* (encoding an inessential 600-aa protein of unknown function) (Figure 1C).

rad24 encodes a 270-aa protein of the 14–3–3 protein family. The 14–3–3 proteins are highly conserved and broadly distributed in eukaryal taxa, which often have multiple 14–3–3 paralogs in their proteomes. Adopting a W-shaped homodimeric quaternary structure, 14–3–3 proteins bind to (and regulate the location and/or function of) a variety of cellular phosphoproteins (44,45). Whereas fission yeast Rad24 is inessential for vegetative growth, a simultaneous deletion of Rad24 and its 14–3–3 paralog Rad25 is lethal (46). It had been shown previously that *rad24Δ* cells exhibit increased acid phosphatase activity and *pho1* transcript levels, whereas Pho1 expression was unaffected in *rad25Δ* cells (47). The *ADS-1* mutation isolated presently is located within the 5'-UTR of the *rad24* transcription unit and results in the creation of a new ATG start codon upstream of the Rad24 polypeptide start site (Figure 1C and Supplementary Figure S1A). This new ATG establishes a 17-aa upstream ORF in the 5'-UTR that overlaps the native Rad24 start site (Supplementary Figure S1A). It is predicted that ribosome scanning and translation of the upstream overlapping ORF will strongly repress the translation of the Rad24 polypeptide (48).

ADS mutations de-repress acid phosphatase expression in a wild-type *asp1*⁺ background

We crossed the *ADS* strains, in which the *asp1* locus was replaced by a G418-resistance marker, with a wild-type strain in which the *asp1-WT* allele was flanked by a hygromycin-resistance marker. The G418/hygromycin-resistant diploids were sporulated and >1000 haploid progeny were selected for the resistance markers linked to the *asp1Δ* and *asp1-WT* alleles. *asp1-WT* colonies were screened for acid phosphatase expression by agar overlay, with deep red color indicating presence of the *ADS* mutation. About half of the *asp1-WT* progeny from the *ADS* backcrosses were lightly stained red (i.e. reflecting the fact that the basal level of 'repressed' Pho1 activity in *asp1-WT* cells is several fold higher than the 'hyper-repressed' Pho1 state in *asp1Δ* cells) and half were darker red. Focused sequencing of the *ADS* loci in individual darker red *ADS asp1-WT* haploids affirmed the presence of the *ADS* mutations. Focused sequencing of the *pom1* locus and the *gsa1* locus in the *ADS-1 asp1-WT* strain showed that the *pom1* nonsense mutation had been eliminated during the cross to wild-type but the *gsa1* missense mutation was retained. Sequencing of the *tif452* locus in the *ADS-5 asp1-WT* strain showed that the *tif452* splice site mutation had been eliminated during the cross to wild-type. Spot tests of growth of the five *ADS asp1-WT* strains on YES agar is shown in Supplementary Figure S4A. The *ADS-1*, *ADS-3*, and *ADS-4* strains grew well at all temperatures. *ADS-2* grew well at 30°C and 34°C, slowly at 37°C and 25°C, and poorly at 20°C, as gauged by colony size. The *ADS-5 asp1-WT* strain was sick at all temperatures.

The *ADS asp1-WT* strains were grown in phosphate-replete medium at 30°C and assayed for acid phosphatase

activity. The *ADS-1*, *ADS-2*, *ADS-3*, *ADS-4*, and *ADS-5* mutations increased acid phosphatase expression by 13-fold, 6-fold, 4-fold, 3-fold, and 4-fold, respectively, *vis-à-vis* the *asp1*⁺ wild-type control (Supplementary Figure S4B). Acid phosphatase activity in *ADS-1* cells was 10-fold higher in the *asp1-WT* background than in the *asp1Δ* background (Supplementary Figure S4B versus 1B), signifying that de-repression of acid phosphatase expression by the *rad24* 5'-UTR mutation is enhanced by *Asp1*. By contrast, acid phosphatase activities in *ADS-2*, *ADS-3*, *ADS-4*, and *ADS-5* cells were only 3-fold, 2-fold, 2-fold, and 1.5-fold higher in the *asp1-WT* context, respectively, than in the *asp1Δ* context.

In order to determine whether the increased acid phosphatase activity in the *asp1-WT ADS-1*, *ADS-2*, *ADS-3* and *ADS-4* strains was caused by increased expression of the thiamine-repressible *pho4* gene, or the *pho1* gene, or both, we mated them to a *pho4Δ* strain and a *pho1Δ* strain, selected haploid progeny for the nourseothricin-resistance or *ura4*⁺ markers used to delete *pho4* and *pho1*, respectively, and then screened by PCR and sequencing for the respective *ADS* alleles. The *pho1Δ* allele eliminated nearly all of the basal level of cell surface-associated acid phosphatase activity from fission yeast grown in phosphate-replete medium. The *pho4Δ* allele had no effect on acid phosphatase activity (Supplementary Figure S5), because Pho4 expression is repressed under such growth condition by the available thiamine. We found that deletion of *pho1* effaced the increased acid phosphatase activity in the *ADS-1* and *ADS-2* strains, whereas deletion of *pho4* did not (Supplementary Figure S5). By contrast, when *ADS-3* and *ADS-4* strains (bearing mutations affecting thiamine biosynthetic enzymes) were crossed to *pho4Δ* and *pho1Δ* mutants, the increased acid phosphatase activities were diminished by deletion of either *pho1* or *pho4*, it being the case that *pho4Δ* exerted a greater decrement in acid phosphatase activity than did *pho1Δ* in the *ADS-3* and *ADS-4* mutants (Supplementary Figure S5). Because the goal of our *ADS* screen was to identify novel mutations affecting lncRNA regulation of *pho1* expression, the focus of our subsequent experiments will be on *rad24*, the gene mutated in *ADS-1*.

De-repression of *pho1* expression by *rad24Δ* depends on CPF subunits, Rhn1, and Pin1

We constructed a fission yeast *rad24Δ* strain, which grew on YES agar at 20–37°C, albeit with colony size slightly smaller than wild-type (Figure 2A). To test genetically if loss of Rad24 de-represses *pho1* via precocious termination of transcription of the interfering *pri* lncRNA, we introduced the *rad24Δ* mutation into knockout strains lacking the Dis2, Ctf1, Ppn1, or Swd22 subunits of the fission yeast cleavage and polyadenylation factor complex CPF (49), a strain with a catalytically dead (C13S) version of the Ssu72 protein phosphatase subunit of CPF, and a strain that lacks the transcription termination factor Rhn1 (10). We also combined *rad24Δ* with a knockout of the Pin1 peptidyl-prolyl isomerase. Pin1 is a positive effector of 3'-processing/termination that acts via Ssu72 (50). Viable double-mutant haploids were recovered after pairwise mating and sporulation of the diploids. Spot tests of growth

between biological replicates (Pearson coefficients of 0.985–0.990). A cutoff of ± 2 -fold change in normalized transcript read level and an adjusted *P*-value of ≤ 0.05 were the criteria applied to derive an initial list of differentially expressed annotated loci in the *rad24* Δ mutant versus the wild-type control. We then focused on differentially expressed genes with average normalized read counts ≥ 100 in either the mutant or wild-type strain in order to exclude transcripts that were expressed at very low levels in vegetative cells. We thereby identified sets of 204 and 194 annotated protein-coding genes that were respectively up-regulated and down-regulated by these criteria in *rad24* Δ cells (Supplementary Table S2). The upregulated mRNAs included those of phosphate homeostasis genes *tgp1* (up 25-fold) and *pho1* (up 10-fold) and of the *ecl3* gene (up 11-fold) located immediately upstream of the tandem *pho84-pho1* locus. The *rds1* gene, which is known to be repressed under phosphate-replete conditions and de-repressed by phosphate starvation (51), was up by 12-fold in *rad24* Δ cells. Consistent with the known role of Rad24 in restricting the activity of the central meiotic transcription factor Ste11 (52) and the propensity of a *rad24* null mutant to mate without nutrient starvation (53), we observed that multiple mRNAs associated with mating and meiosis were upregulated in *rad24* Δ cells, including: *map2* (up 87-fold); *mug14* (up 77-fold); *mug108* (up 26-fold); *spn6* (up 16-fold); *spo13* (up 11-fold); *mei2* (up 8-fold); *map4* (up 7-fold); *map3* (up 7-fold); *mfm2* (up 5-fold); and *map1* (up 2-fold). Overexpression of mRNA encoding the cell surface adhesion protein Map4 might account for the ‘clumping’ phenotype displayed by *rad24* Δ cells during vegetative growth. Several genes of the fission yeast iron homeostasis regulon (54,55) were up-regulated in *rad24* Δ cells, including: *fiol1* (up 6-fold); *fipl1* (up 5-fold); *str1* (up 5-fold); *srx1* (up 3-fold); and *frp2* (up 2-fold).

De-repression of *pho1* expression by *rad24* Δ ensues from squelching the production of interfering *prt* lncRNA

The *prt* lncRNA derived from the chromosomal *prt-pho1* locus in logarithmically growing vegetative cells is rapidly degraded by the nuclear exosome under the direction of DSR (determinant of selective removal) elements in the *prt* RNA (8,56,57). However, increasing the gene dosage of the *prt-pho1* locus (depicted in Figure 3A) by placing it on a multicopy reporter plasmid in *pho1* Δ cells has permitted the analysis of internally terminated *prt* transcripts by Northern blotting and the identification of two internal *prt* poly(A) sites, PAS and PAS2, by 3'-RACE (10). The *prt* locus gives rise to three classes of poly(A)⁺ RNA: (i) a ~ 2.5 kb RNA corresponding to a *prt-pho1* read-through transcript, this being the lncRNA that interferes with *pho1* mRNA synthesis; (ii) a ~ 0.4 kb species, *prt* PAS, that corresponds to *prt* RNA that was cleaved and polyadenylated at the +351 PAS site and (iii) a ~ 0.6 kb species, *prt* PAS2, that corresponds to *prt* RNA that was cleaved and polyadenylated at the +589 PAS2 site (Figure 3A). These three classes of transcript are seen in a Northern blot of RNAs isolated from three independent cultures of *rad24-WT pho1* Δ cells bearing the *prt-pho1* reporter plasmid (Figure 3B, lanes WT). We find that production of the *prt-pho1* read-through transcript is strongly squelched in

reporter-bearing *rad24* Δ cells, whereas the internally terminated transcripts are comparatively spared (Figure 3B, lanes *rad24* Δ). This result is consistent with the idea that absence of Rad24 enhances the propensity of Pol2 to terminate *prt* transcription prior to traversal of the *pho1* gene. Yet, it is not the case that the decrement in the long *prt-pho1* read-through transcript in *rad24* Δ cells is accompanied by an increase in the steady-state levels of the short *prt* PAS and *prt* PAS2 RNAs. It is conceivable that *rad24* Δ elicits termination/polyadenylation at diffuse sites within the *prt* gene (precluding detection as discrete species on a Northern blot) or that the absence of Rad24 promotes turnover of transcripts precociously terminated at PAS and PAS2. The effects of *rad24* Δ on the *prt* transcripts are virtually identical to those reported previously for the IPP pyrophosphatase-defective *asp1-H397A* mutant strain (11).

The plasmid-borne *prt-pho1* reporter faithfully reflects the previously described homeostatic controls on the native *pho1* locus (8,11,58). Here we found that the *prt-pho1* reporter was responsive to ablation of Rad24, whereby Pho1 acid phosphatase activity of phosphate-replete wild-type *rad24*⁺ cells (33.3 ± 1.2) was de-repressed by 12-fold in *rad24* Δ cells (399 ± 11) (Figure 4A). Northern blotting with an mRNA-specific probe revealed two transcripts derived from the *pho1* reporter in *rad24-WT* cells: a ~ 1.6 -kb *pho1* mRNA and a longer *prt-pho1* lncRNA (Figure 3B). The *rad24* Δ mutation curtailed production of the interfering lncRNA and increased the level of the *pho1* mRNA (Figure 3B). Scanning the blot with a phosphorimager and analysis of the signal intensities in ImageQuant showed that *rad24* Δ de-repressed *pho1* mRNA by 14-fold.

De-repression of *pho1* by *rad24* Δ depends on DSR elements in the *prt* lncRNA

The *prt* lncRNA contains two clusters of DSR elements (Figure 3A, denoted by blue boxes), each composed of three DSR hexanucleotide elements. The DSR clusters in the nascent lncRNA are binding sites for Mmi1 (8,59). Previous studies underscored the role of the DSR clusters in *prt*-promoted *pho1* repression, by surveying the effects of compound mutations introduced into each of the hexanucleotide motifs comprising the DSR sequences of the *prt-pho1* reporter plasmid (8,10). Mutating the distal DSR cluster reduced Pho1 expression by 5-fold; mutating the upstream DSR cluster reduced Pho1 expression by half (8). Mutating both DSR clusters reduced Pho1 expression to 10% of the level achieved with the wild-type *prt-pho1* reporter (Figure 4A). The hyper-repressive effect of the *prt* DSR mutations on Pho1 expression were shown previously to ‘win out’ over the de-repressive effects of *CTD-S7A*, *asp1-H397A* (increased IP8), and *erh1* Δ , suggesting that DSRs are key to establish the precocious termination of *prt* lncRNA synthesis that underlies Pho1 de-repression (8,11,58). Here we found that the DSR mutations reduced Pho1 expression in *rad24* Δ cells to 3% of the wild-type DSR reporter control (Figure 4A). We conclude that *rad24* Δ de-repression of *pho1* is contingent on the DSR elements in the *prt* lncRNA.

A *prt*-probed Northern blot of RNAs isolated from three independent cultures of *rad24-WT pho1* Δ and *rad24* Δ

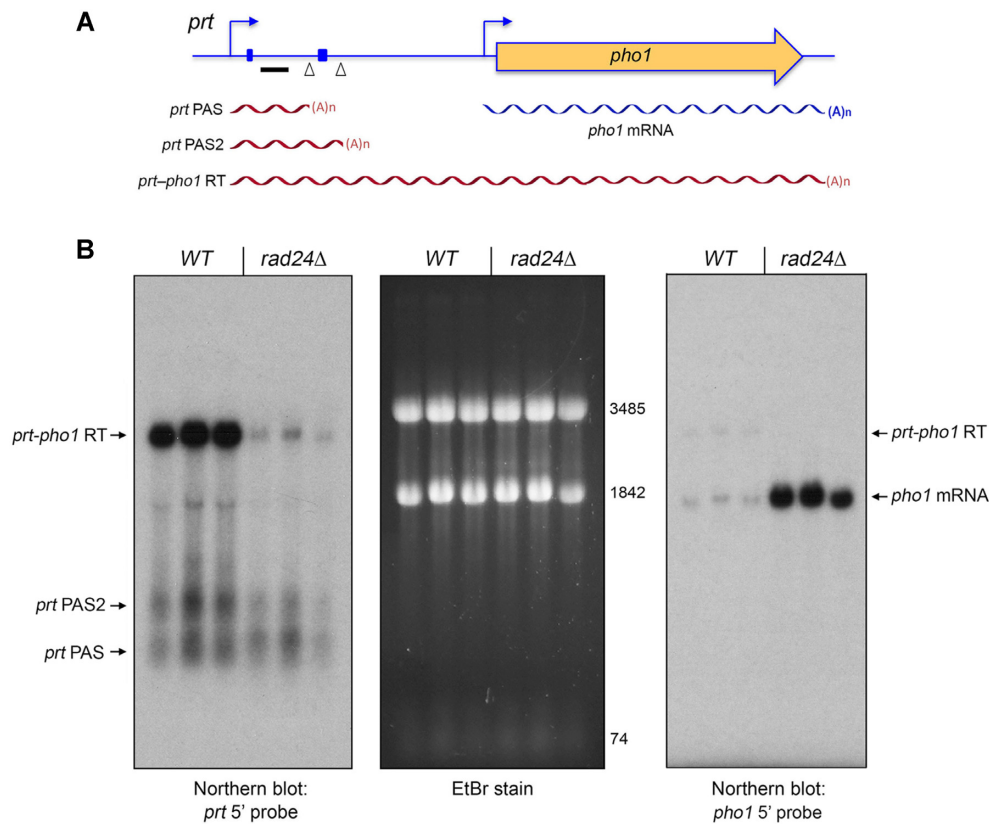


Figure 3. De-repression of *pho1* expression by *rad24* Δ ensues from squelching the production of interfering *prt* lncRNA. (A) Schematic of the *prt-pho1* locus in the reporter plasmid. Transcription start sites are indicated by bent blue arrows. Triangles denote internal poly(A) sites PAS and PAS2. DSR element clusters are indicated by small blue boxes. The gene-specific probe for *prt* (a 32 P-labeled ssDNA complementary to the segment of the *prt* RNA from nucleotides +160 to +202) is denoted by a horizontal black bar. Three classes of poly(A)⁺ *prt* transcripts are depicted as red wavy lines below the *prt-pho1* locus. (B) RNA was isolated from three independent cultures of *pho1* Δ cells bearing the *prt-pho1* reporter plasmid; the cells were either wild-type with respect to *rad24*⁺ or *rad24* Δ as specified. The RNAs were resolved by formaldehyde-agarose gel electrophoresis and stained with ethidium bromide to visualize 28S and 18S ribosomal RNAs (3485 and 1842 nucleotides, respectively) and tRNAs (74 nucleotides) (middle panel). The RNAs in the gel were transferred to a membrane and hybridized to the *prt* probe (left panel) and *pho1* mRNA probe (right panel). Annealed probe was visualized by autoradiography. The three classes of *prt* transcripts are indicated on the left.

pho1 Δ cells bearing the DSR mutant *prt-pho1* reporter plasmid is shown in Figure 4B. As reported previously (10), compared to the *prt* signal of wild-type cells bearing the wild-type reporter (analyzed in parallel), we see that mutation of the DSRs stabilized the *prt-pho1* read-through transcript and the *prt* PAS2 transcript, thereby increasing their steady-state levels (Figure 4B). The salient finding was that the squelching of the *prt-pho1* read-through transcript by *rad24* Δ was prevented by DSR mutation (Figure 4B). The RNA analysis affirms the inferences from Pho1 activity assays that de-repression of *pho1* by *rad24* Δ requires the *prt* lncRNA DSRs. The level of the *prt* PAS transcript derived from the DSR mutant reporter plasmid was slightly higher in *rad24* Δ versus *rad24*-WT cells, consistent with the idea that *rad24* Δ elicits precocious 3'-processing (Figure 4B).

Effect of *prt* lncRNA PAS mutations on *prt-pho1* reporter activity in *rad24* Δ cells

3'-processing of nascent *prt* lncRNA at PAS and PAS2 via the canonical poly(A) pathway will terminate *prt* transcription upstream of the Pho7 binding sites in the *pho1* mRNA promoter and thus alleviate transcription interference. PAS

and PAS2 utilization is a tunable influence on *pho1* expression, insofar as: (i) simultaneous nucleobase substitution mutations of the *prt* PAS and PAS2 elements of the *prt-pho1* reporter results in hyper-repression of the flanking *pho1* promoter (10) (Figure 4A); and (ii) dual PAS mutations attenuate the de-repression of Pho1 expression elicited by *CTD-S7A* and *seb1-G476S* alleles (10,14). Here we found that the dual *prt* PAS mutations reduced Pho1 expression in *rad24* Δ cells to 34% of the wild-type PAS reporter control (Figure 4A). The partial attenuation of *rad24* Δ de-repression by elimination of these two poly(A) signals contrasts with the stricter dependence of *rad24* Δ de-repression on the DSR elements, which suggests that there are additional sites of *prt* 3'-processing that come into play in *rad24* Δ cells. A *prt*-probed Northern blot of RNAs from *rad24*-WT *pho1* Δ cells bearing the dual PAS mutant *prt-pho1* reporter plasmid revealed an increase in the steady-state level of the *prt-pho1* read-through transcript compared to the wild-type reporter control, albeit to a lesser extent than the increase seen in the DSR mutant reporter (Figure 4B). The dual PAS mutations ameliorated the squelching of *prt-pho1* read-through by *rad24* Δ (Figure 4B). A long exposure of the blot focused on comparing the *prt* tran-

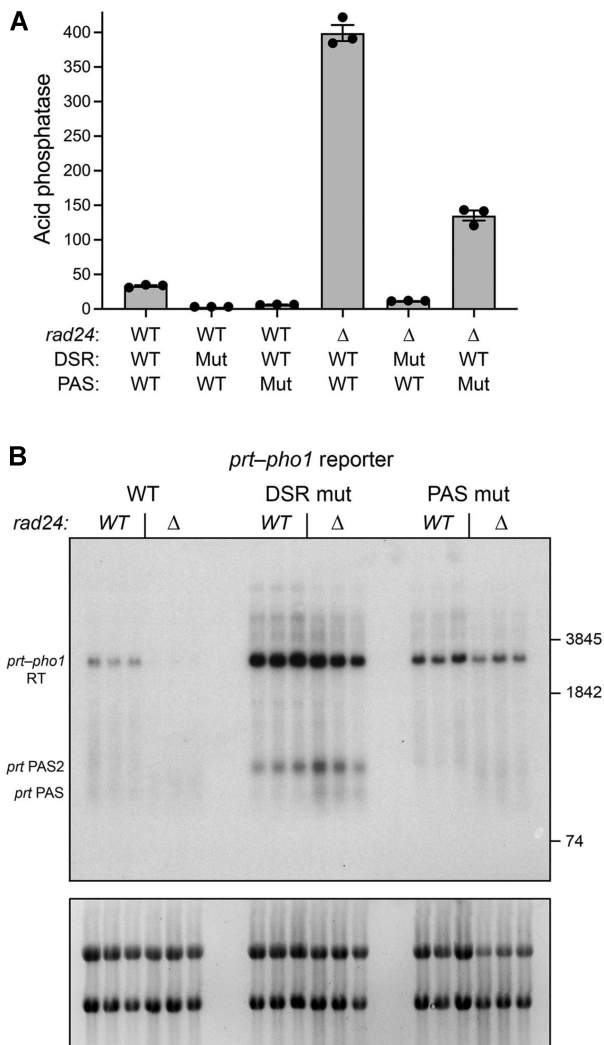


Figure 4. Contribution of DSR elements and poly(A) signals in the *prt* lncRNA to de-repression of *pho1* by *rad24*Δ. (A) *rad24*-WT *pho1*Δ or *rad24*Δ *pho1*Δ cells bearing *prt*-*pho1* reporter plasmids with wild-type or mutated (Mut) DSR clusters and polyadenylation signals (PAS) as indicated were assayed for acid phosphatase activity. (B) RNA isolated from three independent cultures of *rad24*-WT *pho1*Δ or *rad24*Δ *pho1*Δ cells bearing wild-type, DSR mutant or PAS mutant *prt*-*pho1* reporter plasmids was analyzed by Northern blotting using a *prt* 5' probe (top panel). The agarose gel was stained with ethidium bromide to visualize rRNAs prior to transfer of the content to membrane (bottom panel).

scripts from the DSR and PAS mutant reporter plasmids in *rad24*Δ cells indicated that the dual PAS mutation dampened production of the *prt* PAS and *prt* PAS2 lncRNAs and resulted in the appearance of a new *prt* short transcript (denoted by the asterisk in Supplementary Figure S6) migrating between the *prt* PAS and *prt* PAS2 lncRNAs.

De-repression of *pho1* expression by *rad24*Δ depends on Asp1 IPP kinase activity and is enhanced by deletion of Aps1 IPP pyrophosphatase

Genetic manipulation of IPP kinase and IPP pyrophosphatase enzymes have opposite effects on *pho1* expression in phosphate-replete cells (11). Whereas the IPP kinase

dead *asp1*-D333A allele reduces Pho1 acid phosphatase by 10-fold *vis-à-vis* wild-type, the deletion of IPP pyrophosphatase Aps1 increases Pho1 activity by 5-fold (Figure 5B). To gauge the effect of *asp1*-D333A and *aps1*Δ on the de-repression of Pho1 by *rad24*Δ, we constructed double-mutants and tested them for growth (Figure 5A) and acid phosphatase activity (Figure 5B). The *asp1*-D333A allele elicited a 25-fold decrement in the acid phosphatase activity of *rad24*Δ cells. Yet, the low acid phosphatase activity of the *asp1*-D333A *rad24*Δ strain (activity value of 5.6) was still 8-fold greater than that of the hyper-repressed *asp1*-D333A strain. Thus, *rad24*Δ manifests an 'ADS-like' effect on the Asp1 kinase-dead strain akin to that of the *ADS1 rad24* 5'-UTR mutation on the Asp1 deletion strain (Figure 1B). Combining *rad24*Δ with the *aps1*Δ allele had an additive effect of Pho1 de-repression, resulting in an activity value of >200 (Figure 5B), which is the highest we have seen for Pho1 expression from the chromosomal *pho1* locus under phosphate-replete conditions in any fission yeast mutant background. We surmise that IP8 synthesis is required for precocious termination of *pho1*-interfering lncRNA transcription in *rad24*Δ cells and that increasing the level of IP8 by eliminating an IPP pyrophosphatase enhances precocious termination in *rad24*Δ cells. Combining *rad24*Δ with *csk1*Δ (which, *per se*, increased Pho expression by 5-fold) resulted in a level of Pho1 activity intermediate to those of the component single-mutants (Figure 5B), indicating that full de-repression in the absence of Rad24 relies on Csk1 being present.

De-repression of *pho1* by *rad24*Δ depends on Thr4 of the Pol2 CTD

The de-repressive effect of *rad24*Δ on Pho1 expression and its genetic reliance on IP8 synthesis, CPF subunits, Rhn1, and Pin1 reported above is similar to the IP8/CPF/Rhn1/Pin1-dependent de-repression of *pho1* observed in *rbp1*-CTD-*S7A* cells and contrasts with the hyper-repression of Pho1 in *rbp1*-CTD-*T4A* cells (8,10,11,50). Loss of the Thr4 mark is thought to elicit a defect in termination of lncRNA synthesis and results in lethality when combined with mutations in CPF subunits Swd22 and Ppn1 (10). To query epistasis of *rad24*Δ with the Pol2 CTD, we constructed a *CTD*-*T4A rad24*Δ double mutant (Figure 6A). Assays of acid phosphatase activity showed that de-repression of Pho1 by *rad24*Δ was effaced by the *CTD*-*T4A* allele (i.e. Pho1 activity in *T4A rad24*Δ cells was 2% that of *rad24*Δ cells and one-third that of wild-type cells) (Figure 6B). Thus, *T4A* 'wins out' over *rad24*Δ with respect to Pho1 expression, just as it does over other mutations (*CTD*-*S7A*, *asp1*-H397A, *aps1*Δ, *erh1*Δ) that de-repress the *prt*-*pho1* locus (11,58).

The finding that CTD alleles *Y1F*, *S2A*, and *T4A* have overlapping synthetic lethals with CPF mutants *ppn1*Δ and *swd22*Δ suggested that Tyr1-Ser2-Thr4 comprise a three-letter CTD code 'word' that abets termination (10). Therefore, we queried the effect of eliminating the Tyr1 and Ser2 phospho-sites on Pho1 expression in *rad24*Δ cells by constructing *CTD*-*Y1F rad24*Δ and *CTD*-*S2A rad24*Δ double mutants (Figure 6A). Whereas the *Y1F* and *S2A* alleles *per se* did not affect Pho1 activity in

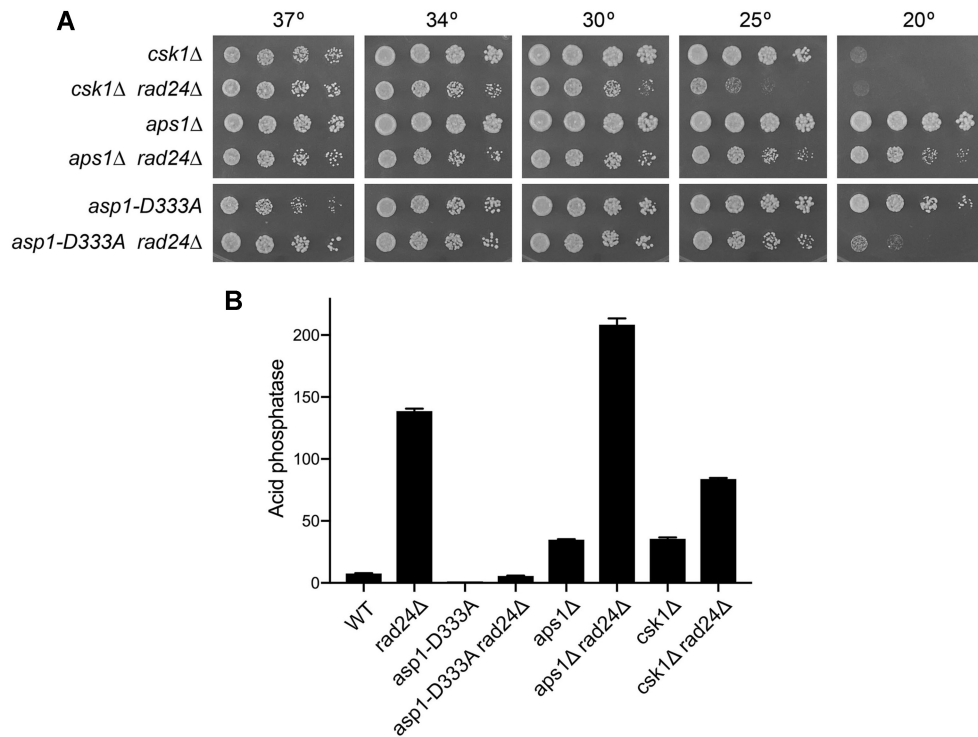


Figure 5. De-repression of *pho1* by *rad24Δ* depends on Aps1 IPP kinase activity and is enhanced by deletion of Aps1 IPP pyrophosphatase. Fission yeast strains bearing the indicated *rad24*, *asp1*, *aps1*, and *csk1* alleles were spot tested for growth on YES agar at the indicated temperatures (panel A) or grown in liquid culture at 30°C and assayed for acid phosphatase activity (panel B).

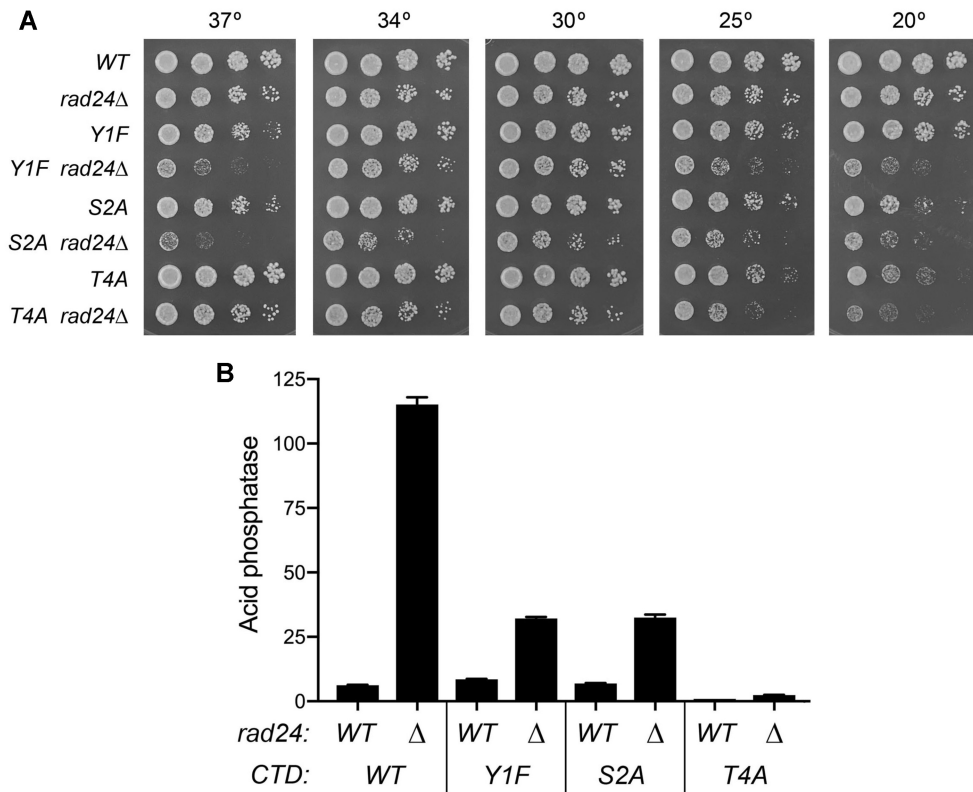


Figure 6. De-repression of *pho1* by *rad24Δ* depends on Thr4 of the Pol2 CTD. *rad24-WT* and *rad24Δ* strains, *rpb1-CTD* -Y1F, -S2A and -T4A mutants, and *rad24Δ* cells bearing *CTD* -Y1F, -S2A, and -T4A alleles were spot tested for growth on YES agar at the indicated temperatures (panel A) or grown in liquid culture at 30°C and assayed for acid phosphatase activity (panel B).

rad24-WT cells, they did attenuate the Pho1 de-repression elicited by *rad24Δ*, such that acid phosphatase activity in the *Y1F rad24Δ* and *S2A rad24Δ* strains was 28% that of the *rad24Δ* single mutant (Figure 6B).

***rad24Δ asp1-H397A* growth defect is rescued by CPF, Rhn1, Pin1, and CTD mutations**

The IPP pyrophosphatase-dead H397A mutation of the bifunctional Asp1 IPP kinase-pyrophosphatase enzyme elicits a stronger de-repression of *pho1* than a deletion of the Nudix pyrophosphatase Aps1 (11). Our attempt here to construct a *rad24Δ asp1-H397A* strain yielded double-mutant haploids that germinated and grew out very slowly after sporulation, grew poorly in liquid YES medium, and did not form macroscopic colonies on YES agar (Figure 7A). In effect, the combination of these two strongly *pho1* de-repressive alleles was synthetically near-lethal. A key question is whether the severe sickness of *rad24Δ asp1-H397A* arises from unconstrained precocious transcription termination. If so, then we might expect the synthetic growth defect would be ameliorated by mutations in the 3'-processing/termination machinery or the Pol2 CTD. To test this idea, we crossed *rad24Δ* with *asp1-H397A ppn1Δ*, *asp1-H397A swd22Δ*, *asp1-H397A dis2Δ*, *asp1-H397A ctf1Δ*, *asp1-H397A ssu72-C13S*, *asp1-H397A pin1Δ*, *asp1-H397A rhn1Δ*, *asp1-H397A CTD-T4A*, and *asp1-H397A CTD-Y1F* and screened random spores for each of the differentially marked loci of interest. In this way, we recovered viable *rad24Δ asp1-H397A* haploids bearing loss-of-function alleles of CPF subunits, Pin1, and Rhn1 and the Pol2 CTD-T4A and CTD-Y1F alleles. Spot tests of the triple-mutants for growth on YES agar at 30°C showed that their colony size and number was similar to that of the *rad24Δ* strain (Figure 7A).

The triple mutants were assayed for Pho1 activity in parallel with the *rad24Δ* and *asp1-H397A* single-mutants (Figure 7B). Whereas loss of CPF subunits Dis2 and Ctf1 restored viability of *rad24Δ asp1-H397A* cells, the expression of Pho1 acid phosphatase was extremely elevated (higher than in the *rad24Δ* strain). By contrast, deletion or loss-of-function mutations of Ppn1, Swd22, Ssu72, Pin1, and Rhn1, and the CTD-T4A mutation exerted stronger effects in reducing Pho1 expression to levels similar to, or below, that of the *asp1-H397A* single mutant strain (Figure 7B). The CTD-Y1F allele reduced Pho1 expression to a level between that of *asp1-H397A* and *rad24Δ* single mutant cells.

Spontaneous mutations in Ctf1 and Ssu72 suppress the *rad24Δ asp1-H397A* growth defect

To further probe the basis for the severe growth defect of *rad24Δ asp1-H397A* cells, we isolated spontaneous *SRA* (Suppressor of Rad24 Asp1) mutants that gave rise to rare larger colonies when the *rad24Δ asp1-H397A* strain was plated on YES agar at 30°C. We picked two candidate suppressor mutants—*SRA-1* and *SRA-2*—which, after isolation of a single colony and amplification in liquid culture, yielded a homogeneous population of larger-than-parental colonies. The *SRA* mutants grew similarly to the *rad24Δ*

single mutant at 20–34°C but were sick at 37°C (Figure 8A). Whole genome sequencing of the *SRA-1* and *SRA-2* strains and comparison to the genomes of the parental *rad24Δ* and *asp1-H397A* mutants affirmed that the original *rad24Δ* and *asp1-H397A* loci were unchanged in *SRA-1* and *SRA-2* and identified a single, apparently causative, suppressor mutation in each strain. *SRA-1* cells bore a nonsense mutation in the *ctf1* gene that truncated the 363-aa Ctf1 protein at Tyr260. *SRA-2* cells had a nonsense mutation in the *ssu72* gene that truncated the 197-aa Ssu72 polypeptide at Gln67 (Figure 8C). Pho1 expression in *SRA-1* cells exceeded that in *rad24Δ* cells, whereas Pho1 expression in the *SRA-2* strain was similar to that of *asp1-H397A* cells (Figure 8B). That an unbiased suppressor screen returned loss-of-function mutations in two different subunits of the CPF complex fortifies the conclusion that the toxic effect of *rad24Δ asp1-H397A* is exerted at the level of RNA 3'-processing/termination.

rad24Δ* is synthetically lethal with *erh1Δ

Fission yeast Erh1 exists in a complex with Mmi1, the RNA-binding protein that recognizes the DSR elements in *pri* and other lncRNAs, recruits CPF, and promotes lncRNA transcription termination (8,60,61). Deletion of *erh1* de-represses *pho1* via precocious 3'-processing/termination of *pri* lncRNA synthesis (58). *pho1* de-repression by *erh1Δ* depends on CPF/Rhn1, Asp1 IPP kinase activity, the Thr4 CTD mark, and the DSR clusters in the *pri* lncRNA (58). It is proposed that Erh1 acts as a brake on Mmi1's ability to promote CPF-dependent termination during *pri* lncRNA synthesis, such that when Erh1 is absent Mmi1 is unrestrained in eliciting precocious *pri* termination and thus de-repression of *pho1* mRNA synthesis. Given the similar genetic requirements for *pho1* de-repression by *rad24Δ* and *erh1Δ*, we queried possible mutational synergies by mating *rad24Δ* and *erh1Δ* strains, sporulating the heterozygous diploids, and screening a large random population of haploid progeny for the drug-resistance markers linked to the *rad24Δ* and *erh1Δ* loci. Failure to recover any viable *rad24Δ erh1Δ* double-mutants (while recovering wild-type and single mutants at the expected frequencies) signified that *rad24Δ* is synthetically lethal with *erh1Δ*, most likely via exuberant precocious termination affecting the expression of one or more essential fission yeast genes.

Effect of mutating the phosphoprotein binding site of Rad24

Alignment of the amino acid sequence of Rad24 to that of its paralog Rad25 (Figure 9A) highlighted 207 positions of side chain identity/similarity within the N-terminal 240-aa of Rad24. By contrast, the C-terminal 30-aa segments of the paralogs are quite divergent, with only 6 positions of identity/similarity (Figure 9A). We submitted the Rad24 amino acid sequence to the Phyre2 structure modeling server (62), which returned a 'top hit' tertiary structure model templated on the crystal structure of a *Nicotiana tabacum* 14–3–3 protein (pdb 3E6Y; 63). The homology of the tobacco 14–3–3 protein structure to Rad24 spans Rad24 amino acids 4–236. Alignment of the 3E6Y primary

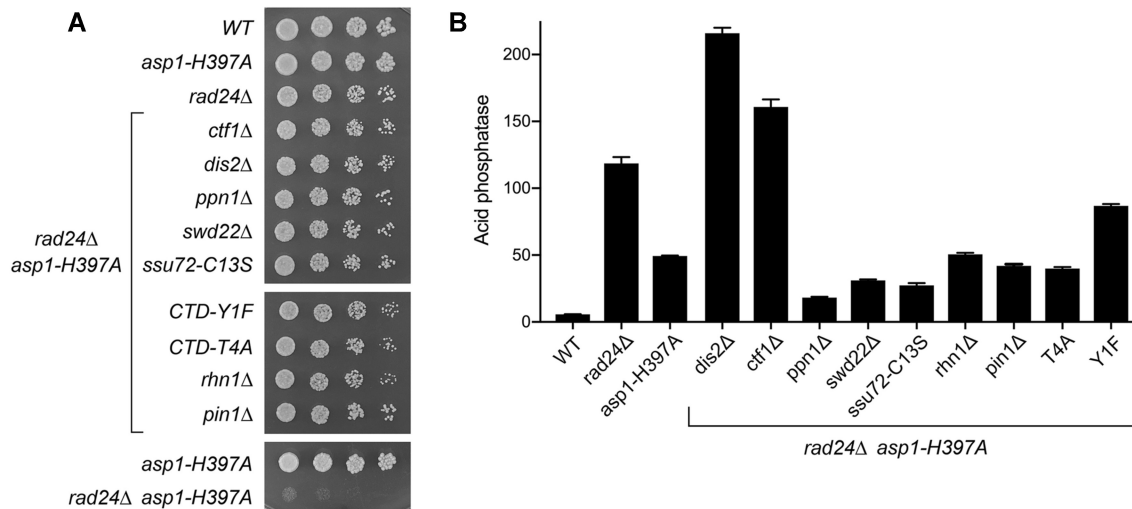


Figure 7. *rad24Δ asp1-H397A* growth defect is rescued by CPF, Rhn1, Pin1, and CTD mutations. Fission yeast strains with genotypes indicated on the left were spot tested for growth on YES agar at 30°C (panel A) or grown in liquid culture at 30°C and assayed for acid phosphatase activity (panel B).

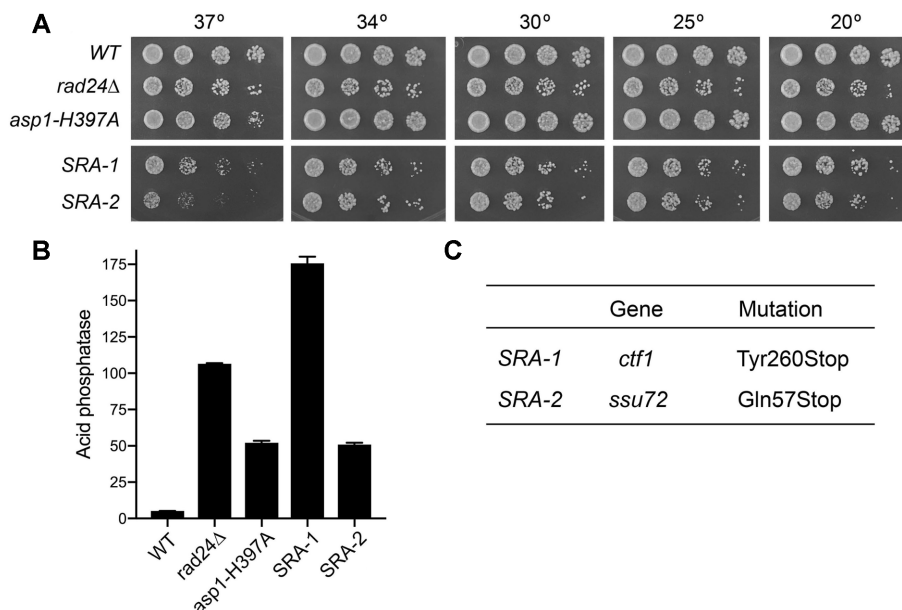


Figure 8. Spontaneous mutations in Ctf1 and Ssu72 suppress the *rad24Δ asp1-H397A* growth defect. (A) Serial 5-fold dilutions of the indicated strains were spotted on YES agar and grown at the indicated temperatures. (B) *SRA-1* and *SRA-2* cells were assayed for Pho1 activity in parallel with wild-type, *rad24Δ*, and *asp1-H397A* controls. (C) Whole-genome sequencing of *SRA-1* and *SRA-2* strains revealed the indicated genetic mutations.

structure to those of Rad24 and Rad25 highlights 181 positions of side chain identity/similarity in all three polypeptides (Figure 9A). The phosphothreonine-binding pocket of 3E6Y is composed of two conserved arginines and a tyrosine (shaded in cyan in Figure 9A) that make atomic contacts to the three non-bridging phosphate oxygens of Thr-PO₄, as shown in Figure 9B, in which the phosphate-binding arginines and tyrosine are labeled according to their position in Rad24. A salient question is whether the de-repression of Pho1 expression *in vivo* seen in the absence of Rad24 can be phenocopied by loss of the atomic contacts to phosphate in the context of an otherwise intact Rad24 protein. To address this issue, we replaced the

wild-type *rad24* chromosomal locus with a mutant allele in which Arg132 and Tyr133 were replaced by alanine or a mutant in which Arg59, Arg132, and Tyr133 were replaced by alanine. We also constructed a strain in which the native *rad24* locus was replaced by a truncated allele *rad24-ΔC* encoding Rad24-(1–240). The *rad24-(R132A-Y133A)*, *rad24-(R59A-R132A-Y133A)* and *rad24-ΔC* strains were assayed for Pho1 activity in parallel with isogenic wild-type and *rad24Δ* controls. The instructive findings were that severance of the phosphate contacts to the arginine and tyrosine side chains phenocopied Rad24 deletion with respect to de-repression of Pho1 expression, whereas deleting the 30-aa C-terminal Rad24 peptide had no effect on Pho1

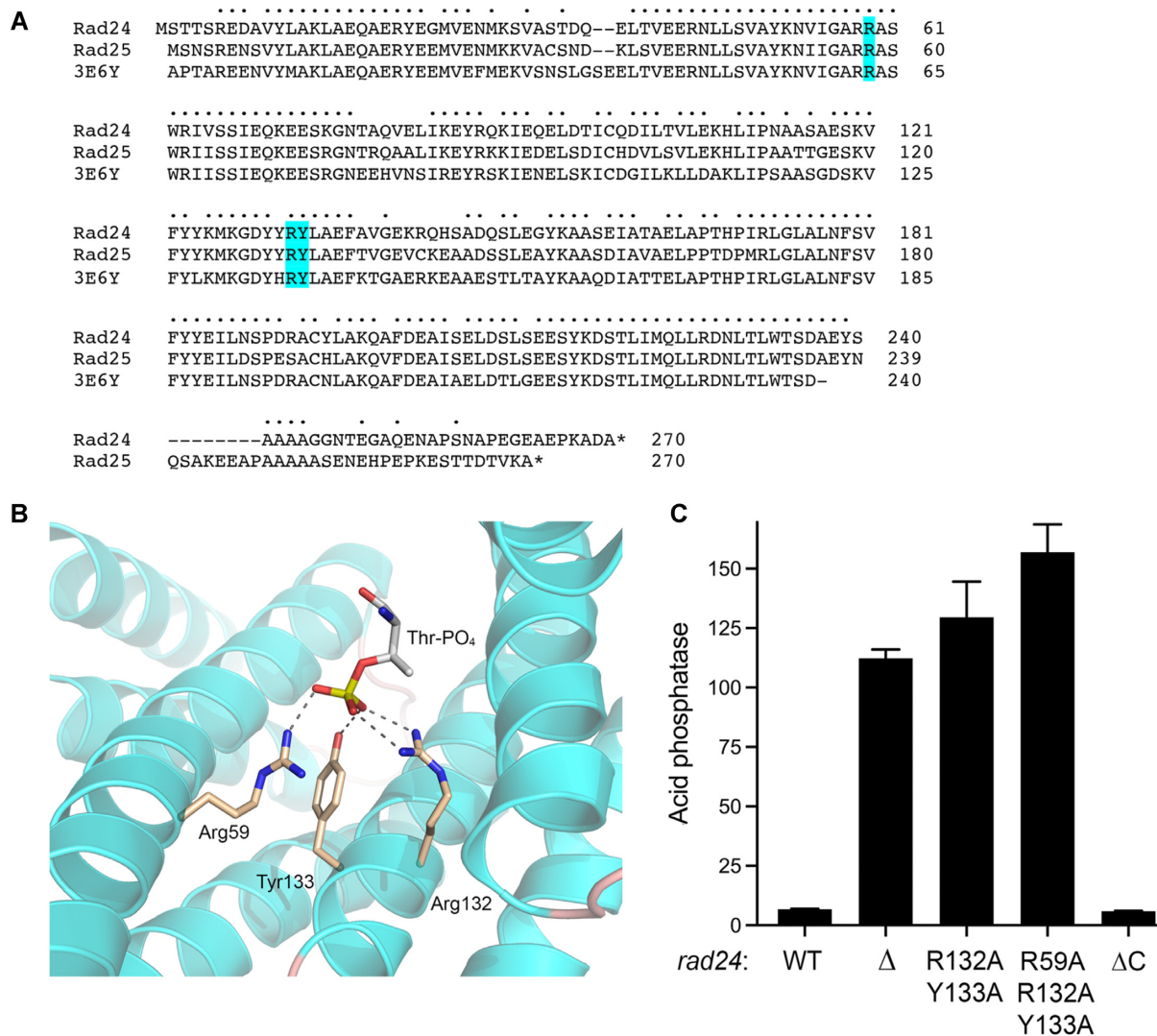


Figure 9. Effect of mutating the phosphoprotein binding site of Rad24. (A) The complete amino acid sequence of fission yeast Rad24 is aligned to that of its paralog Rad25 and to that of a homologous *Nicotiana tabacum* 14–3–3 protein (3E6Y) for which a crystal structure had been determined in complex with a phosphothreonine-containing peptide. Positions of amino acid side chain identity/similarity in all three proteins are denoted by dots above the alignment, as are conserved positions in the C-terminal tails of Rad24 and Rad25. Gaps in the alignment are indicated by dashes. Amino acids that engage the phosphate moiety of phosphothreonine are highlighted in cyan. (B) Structure of the phosphothreonine-binding pocket of 3E6Y. Two conserved arginines and a tyrosine that make atomic contacts (dashed lines) to the three non-bridging phosphate oxygens of Thr-PO₄ (stick model with gray carbons) are depicted as stick models with beige carbons and labeled according to their position in Rad24. (C) *rad24*-(R132A-Y133A), *rad24*-(R59A-R132A-Y133A), and *rad24*-ΔC cells were assayed for Pho1 activity in parallel with isogenic wild-type and *rad24*Δ controls.

expression *vis-à-vis* the wild-type control (Figure 9C). To affirm that mutating the phosphopeptide-binding site did not adversely affect Rad24 protein expression, we replaced the native *rad24* allele with TAP-tagged versions in which the TAP-tag was appended to the C-terminus of wild-type Rad24 protein or the Rad24-(R59A-R132A-Y133A) mutant. Acid phosphatase assays verified that Pho1 was depressed in *rad24*-(R59A-R132A-Y133A)-TAP cells compared to the *rad24*-WT-TAP control (Supplementary Figure S7A). Western blotting of whole cell extracts with IgG (which recognizes the protein A domain of the TAP tag) revealed comparable steady-state levels of appropriately sized wild-type Rad24 and Rad24-(R59A-R132A-Y133A) mutant polypeptides (Supplementary Figure S7B).

DISCUSSION

lncRNA-mediated transcriptional interference that underlies repression of fission yeast phosphate homeostasis gene *pho1* is a sensitive read-out of genetic influences on 3'-processing/termination and a powerful tool for discovery of novel regulators of this step of the Pol2 transcription cycle (5,7,10,11,14,58). The present identification of Rad24 in a forward genetic screen for relief of transcriptional interference in an *asp1*Δ background highlights a new layer of control whereby Pol2 termination is antagonized by a 14–3–3 protein. The genetic, transcriptomic, and biochemical evidence for Rad24 as negative actor in 3'-processing/termination is persuasive. To wit: (i) *rad24*Δ de-represses *pho1* and *tgf1*, both of which are subject to

lncRNA-mediated transcriptional interference; (ii) RNA analysis shows that *rad24Δ* squelches production of the *pri-pho1* RT lncRNA responsible for *pho1* repression and (iii) *rad24Δ* de-repression of *pho1* is erased by loss-of-function mutations in CPF subunits, Pin1, and Rhn1.

Our finding that mutating *cis*-acting elements in the *pri* lncRNA either prevent (via DSR mutations) or blunt (via polyadenylation signal mutations) the de-repression of *pho1* by *rad24Δ* fortifies the case that Rad24 exerts its effects at a post-initiation step of lncRNA synthesis. The DSRs recruit Mmi1, a protein that accelerates the turnover of its client transcripts and also elicits transcription termination (59–61). Inactivating the *pri* DSRs in wild-type cells increases both the *pri-pho1* read-through lncRNA that interferes with *pho1* mRNA synthesis and the short *pri2* PAS2 lncRNA. These two transcripts contain the distal DSR cluster, mutation of which exerts the stronger repressive effect on *pho1* compared to the upstream DSR cluster mutation (8). Mutating the DSRs in *rad24Δ* cells reversed the squelching of *pri-pho1* read-through lncRNA synthesis, thereby accounting for the reversal of *Pho1* de-repression. The levels of the short lncRNAs derived from the DSR mutant reporter in *rad24Δ* cells were similar to, or slightly more than, their levels in *rad24-WT* cells. Thus, the DSRs (and, by extension, Mmi1 binding to the DSRs) are not required for 3'-cleavage/polyadenylation of these two short *pri* lncRNAs. The strong DSR requirement for *pho1* de-repression by *rad24Δ* echoes that seen for *erh1Δ* (58). The synthetic lethality of *rad24Δ* with *erh1Δ* point to functional overlap of Rad24 and Erh1 as protectors against overzealous Mmi1- and CPF-dependent transcription termination.

rad24Δ displays a plexus of instructive genetic interactions with two other prominent governors of lncRNA interference: the Pol2 CTD and inositol pyrophosphate (IPP) dynamics. With respect to the CTD, *rad24Δ* de-repression of *pho1* is reversed by a T4A mutation that prevents installation of the Thr4-PO₄ mark and is itself hyper-repressive of the *PHO* regulon. Copious prior genetic evidence implicates Thr4-PO₄ (or the Thr4-OH) as a positive effector of 3'-processing/termination (10), likely by virtue of Thr4-PO₄ function as a component of the CTD-binding site for termination factors Seb1 and Rhn1 (10,64,65). *rad24Δ* de-repression of *pho1* is also attenuated by CTD mutations Y1F and S2A. Genetic evidence implicates Tyr1-Ser2-Thr4 as a three-letter CTD 'word' that abets termination (10). This CTD word is clearly important for the *rad24Δ* phenotype. Most striking is the observation that *rad24Δ* de-repression of *pho1* is strongly dependent on synthesis of IP8 (or 1-IP7) by the Asp1 IPP kinase. IP8 is a metabolite agonist of 3'-processing/termination in fission yeast (11). Deleting Rad24 in tandem with the IPP pyrophosphatase Aps1 (that degrades IP8) has an additive effect on the extent of *pho1* de-repression. Thus, we surmise that metabolite control of 3'-processing/termination by IPPs is highly sensitive to Rad24 status.

The mutational synergies and synthetic genetic interactions of *rad24Δ* suggest that the action of Rad24 in antagonizing termination is not restricted to the lncRNA that controls *pho1*. *rad24Δ* is synthetically near-lethal with the IPP pyrophosphatase-defective *asp1-H397A* allele, which

raises the intracellular level of IP8 (15) and elicits a precocious lncRNA 3'-processing/termination phenotype similar to that of *rad24Δ* (11). These results indicate that elevated IPP concentrations and loss of Rad24 synergize to affect 3'-processing/termination of one or more genes that are essential for fission yeast vegetative growth. That the near lethality of *rad24Δ asp1-H397A* is caused by exuberant 3'-processing/termination is affirmed by our findings that viability of *rad24Δ asp1-H397A* cells is restored by loss-of-function mutations of CPF subunits, Pin1, termination factor Rhn1, and by CTD mutations T4A and Y1F.

Hints to the means by which Rad24 impacts 3'-processing/termination emerge from our finding that alanine mutations of the Arg59, Arg132, and Tyr133 constituents of the Rad24 phosphate-binding site phenocopied *rad24Δ* with regard to *pho1* de-repression. This signifies that Rad24 interaction with a phosphate-containing ligand is necessary for Rad24 activity in averting precocious lncRNA transcription termination. Because 14–3–3 proteins act as phosphoprotein binders, our results lead us to speculate that Rad24 deploys its phosphate binding site to engage the Thr4-PO₄ mark on the Pol2 CTD (essentially as depicted in Figure 9B) and thereby mask recognition of the Thr4-PO₄ mark by the CTD-binding termination factors Rhn1 and/or Seb1. Absence of Rad24 or mutation of its phosphate site would increase access of termination factors to the CTD in the Pol2 elongation complex and thereby enhance termination. This model predicts that the gain in termination function in *rad24Δ* cells would be negated by the *CTD-T4A* allele that erases the Thr4-PO₄ mark, as was observed experimentally.

An alternative scenario is that Rad24 might deploy its phosphate site to bind IP8 and thereby limit its capacity to trigger precocious termination (11). This model predicts that ablation of Rad24 would increase 'available' IP8 and thus promote precocious termination. Sequestration of a portion of the intracellular pool of IP8 by Rad24 could explain why the *pho1* de-repression in *rad24Δ* cells is dependent on IP8 synthesis by the Asp1 kinase. The IPP pyrophosphatase-dead mutation *asp1-H397A*, which is fairly benign *per se*, becomes toxic in a *rad24Δ* background, conceivably because the increased intracellular level of IP8 (15) is no longer buffered by Rad24. A potential caveat is that loss of Rad24 elicited a several-fold increase in *pho1* expression above a very low baseline in *asp1Δ* cells that do not produce IP8 (this being the basis of the *ADS* screen that led us to Rad24). Yet, loss of Asp1 IPP kinase activity results in an increase in the intracellular pool of IP7 (15). We envision that IP7 is a weak agonist of 3'-processing/termination, as well as a potential ligand for Rad24 (especially if IP8 is absent). In that case, loss of Rad24 would elevate available IP7 and lead to the modest de-repression of *pho1* expression seen in *asp1Δ* cells. Another alternative scenario is that Rad24 might bind to and sequester a (hypothetical) phosphorylated nuclear protein that functions as agonist of precocious termination.

In conclusion, the present study unveils a new role for 14–3–3 proteins in cell physiology at the interface of Pol2 transcription termination, IPP signaling and phosphate homeostasis.

DATA AVAILABILITY

The RNA-seq data in this publication have been deposited in NCBI's Gene Expression Omnibus and are accessible through GEO Series accession number GSE164616.

SUPPLEMENTARY DATA

Supplementary Data are available at NAR Online.

FUNDING

NIH [R01-GM134021 to B.S., R35-GM126945 to S.S.]; MSKCC Integrated Genomics Operation Core is funded by NCI Cancer Center Support Grant [P30 CA08748]; Cycle for Survival, and the Marie-Josée and Henry R. Kravis Center for Molecular Oncology. The funders had no role in study design, data collection and analysis, decision to publish, or preparation of the manuscript. The open access publication charge for this paper has been waived by Oxford University Press - *NAR* Editorial Board members are entitled to one free paper per year in recognition of their work on behalf of the journal.

Conflict of interest statement. None declared.

REFERENCES

- Shuman, S. (2020) Transcriptional interference at tandem lncRNA and protein-coding genes: an emerging theme in regulation of cellular nutrient homeostasis. *Nucleic Acids Res.*, **48**, 8243–8254.
- Carter-O'Connell, I., Peel, M.T., Wykoff, D.D. and O'Shea, E.K. (2012) Genome-wide characterization of the phosphate starvation response in *Schizosaccharomyces pombe*. *BMC Genomics*, **13**, 697.
- Schwer, B., Sanchez, A.M., Garg, A., Chatterjee, D. and Shuman, S. (2017) Defining the DNA binding site recognized by the fission yeast Zn₂Cys₆ transcription factor Pho7 and its role in phosphate homeostasis. *mBio*, **8**, e01218-17.
- Garg, A., Goldgur, Y., Schwer, B. and Shuman, S. (2018) Distinctive structural basis for DNA recognition by the fission yeast Zn₂Cys₆ transcription factor Pho7 and its role in phosphate homeostasis. *Nucleic Acids Res.*, **46**, 11262–11273.
- Henry, T.C., Power, J.E., Kerwin, C.L., Mohammed, A., Weissman, J.S., Cameron, D.M. and Wykoff, D.D. (2011) Systematic screen of *Schizosaccharomyces pombe* deletion collection uncovers parallel evolution of the phosphate signal pathways in yeasts. *Euk. Cell*, **10**, 198–206.
- Schwer, B., Bitton, D.A., Sanchez, A.M., Bähler, J. and Shuman, S. (2014) Individual letters of the RNA polymerase II CTD code govern distinct gene expression programs in fission yeast. *Proc. Natl Acad. Sci. U.S.A.*, **111**, 4185–4190.
- Schwer, B., Sanchez, A.M. and Shuman, S. (2015) RNA polymerase II CTD phospho-sites Ser5 and Ser7 govern phosphate homeostasis in fission yeast. *RNA*, **21**, 1770–1780.
- Chatterjee, D., Sanchez, A.M., Goldgur, Y., Shuman, S. and Schwer, B. (2016) Transcription of lncRNA *pri*, clustered *pri* RNA sites for Mmi1 binding, and RNA polymerase II CTD phospho-sites govern the repression of *pho1* gene expression under phosphate-replete conditions in fission yeast. *RNA*, **22**, 1011–1025.
- Sanchez, A.M., Shuman, S. and Schwer, B. (2018) Poly(A) site choice and Pol2 CTD Serine-5 status govern lncRNA control of phosphate-responsive *tgp1* gene expression in fission yeast. *RNA*, **24**, 237–250.
- Sanchez, A.M., Shuman, S. and Schwer, B. (2018) RNA polymerase II CTD interactome with 3' processing and termination factors in fission yeast and its impact on phosphate homeostasis. *Proc. Natl Acad. Sci. U.S.A.*, **115**, E10652–E10661.
- Sanchez, A.M., Garg, A., Shuman, S. and Schwer, B. (2019) Inositol pyrophosphates impact phosphate homeostasis via modulation of RNA 3' processing and transcription termination. *Nucleic Acids Res.*, **47**, 8452–8469.
- Garg, A., Shuman, S. and Schwer, B. (2020) A genetic screen for suppressors of hyper-repression of the fission yeast *PHO* regulon by Pol2 CTD mutation T4A implicates inositol 1-pyrophosphates as agonists of precocious lncRNA transcription termination. *Nucleic Acids Res.*, **48**, 4811–4826.
- Yague-Sanz, C., Vanrobaeys, Y., Fernandez, R., Duval, M., Laroche, M., Beaudoin, J., Berro, J., Labbe, S., Jaques, P.E. and Bachand, F. (2020) Nutrient-dependent control of RNA polymerase II elongation rate regulates specific gene expression programs by alternative polyadenylation. *Genes Dev.*, **34**, 883–897.
- Schwer, B., Garg, A., Jacewicz, A. and Shuman, S. (2021) Genetic screen for suppression of transcriptional interference identifies a gain-of-function mutation in Pol2 termination factor Seb1. *Proc. Natl Acad. Sci. U.S.A.*, **118**, e2108105118.
- Pascual-Ortiz, M., Saiardi, A., Walla, E., Jakopec, V., Künzel, N.A., Span, I., Vangala, A. and Fleig, U. (2018) Asp1 bifunctional activity modulates spindle function via controlling cellular inositol pyrophosphate levels in *Schizosaccharomyces pombe*. *Mol. Cell. Biol.*, **38**, e00047-18.
- Dollins, D.E., Bai, W., Fridy, P.C., Otto, J.C., Neubauer, J.L., Gattis, S.G., Mehta, K.P. and York, J.D. (2020) Vip1 is a kinase and pyrophosphatase switch that regulates inositol diphosphate signaling. *Proc. Natl Acad. Sci. U.S.A.*, **117**, 9356–9364.
- Moreno, S., Klar, A. and Nurse, P. (1991) Molecular genetic analysis of fission yeast *Schizosaccharomyces pombe*. *Methods Enzymol.*, **194**, 795–823.
- Langmead, B. and Salzberg, S. (2012) Fast gapped-read alignment with Bowtie 2. *Nature Methods*, **9**, 357–359.
- Li, H., Handsaker, B., Wysoker, A., Fennell, T., Ruan, J., Homer, N., Marth, G., Abecasis, G. and Durbin, R. (2009) The Sequence Alignment/Map format and SAMtools. *Bioinformatics*, **25**, 2078–2079.
- Li, H. (2011) A statistical framework for SNP calling, mutation discovery, association mapping and population genetical parameter estimation from sequencing data. *Bioinformatics*, **27**, 2987–2993.
- Cingolani, P., Platts, A., Wang, L., Coon, M., Nguyen, T., Wang, L., Land, S.J., Lu, X. and Ruden, D.M. (2012) A program for annotating and predicting the effects of single nucleotide polymorphisms, SnpEff: SNPs in the genome of *Drosophila melanogaster* strain w1118; iso-2; iso-3". *Fly*, **6**, 80–92.
- Herrick, D., Parker, R. and Jacobsen, A. (1990) Identification and comparison of stable and unstable mRNAs in *Saccharomyces cerevisiae*. *Mol. Cell. Biol.*, **10**, 2269–2284.
- Hentges, P., Van Driessche, B., Tafforeau, L., Vandenhoute, J. and Carr, A.M. (2005) Three novel antibiotic marker cassettes for gene disruption and marker switching in *Schizosaccharomyces pombe*. *Yeast*, **22**, 1013–1019.
- Kim, D., Langmead, B. and Salzberg, S.L. (2015) HISAT: a fast spliced aligner with low memory requirements. *Nature Methods*, **12**, 357.
- Anders, S., Pyl, P.T. and Huber, W. (2015) HTSeq—a Python framework to work with high-throughput sequencing data. *Bioinformatics*, **31**, 166–169.
- Love, M.I., Huber, W. and Anders, S. (2014) Moderated estimation of fold change and dispersion for RNA-seq data with DESeq2. *Genome Biology*, **15**, 550.
- Schweingruber, M.E., Schweingruber, A.M. and Schüpbach, M.E. (1982) Isolation and characterization of acid phosphatase mutants in *Schizosaccharomyces pombe*. *Current Genetics*, **5**, 109–117.
- Maundrell, K., Nurse, P., Schönholzer, F. and Schweingruber, M.E. (1985) Cloning and characterization of two genes restoring acid phosphatase activity in *pho1*-mutants of *Schizosaccharomyces pombe*. *Gene*, **39**, 223–230.
- Schweingruber, M.E., Edenharter, E., Zurlinden, A. and Stockmaier, K.M. (1992) Regulation of *pho1*-encoded acid phosphatase of *Schizosaccharomyces pombe* by adenine and phosphate. *Curr. Genet.*, **22**, 289–292.
- Fankhauser, H., Zurlinden, A., Schweingruber, A.M., Edenharter, E. and Schweingruber, M.E. (1995) *Schizosaccharomyces pombe* thiamine pyrophosphokinase is encoded by gene *tmr3* and is a regulator of thiamine metabolism, phosphate metabolism, mating, and growth. *J. Biol. Chem.*, **270**, 28457–28462.
- Estill, M., Kerwin-Iosue, C.L. and Wykoff, D.D. (2015) Dissection of the *PHO* pathway in *Schizosaccharomyces pombe* using epistasis and the alternate repressor adenine. *Curr. Genet.*, **61**, 175–183.

32. Schweingruber, M.E., Fluri, R., Maundrell, K., Schweingruber, A.M. and Dumermuth, E. (1986) Identification and characterization of thiamin repressible acid phosphatase in yeast. *J. Biol. Chem.*, **261**, 15877–15882.
33. Yang, J.W. and Schweingruber, M.E. (1990) The structural gene coding for thiamin-repressible acid phosphatase in *Schizosaccharomyces pombe*. *Curr. Genet.*, **18**, 269–272.
34. Schweingruber, A.M., Dlugonski, J., Edenharter, E. and Schweingruber, M.E. (1991) Thiamine in *Schizosaccharomyces pombe*: dephosphorylation, intracellular pool, biosynthesis and transport. *Curr. Genet.*, **19**, 249–254.
35. Schweingruber, A.M., Fankhauser, H., Dlugonski, J., Steinmann-Loss, C. and Schweingruber, M.E. (1992) Isolation and characterization of regulatory mutants from *Schizosaccharomyces pombe* involved in thiamine-regulated gene expression. *Genetics*, **130**, 445–449.
36. Timm, D.E., Liu, J., Baker, L.J. and Harris, R.A. (2001) Crystal structure of thiamin pyrophosphokinase. *J. Mol. Biol.*, **310**, 195–204.
37. Goyer, A., Hasnain, G., Frelin, O., Ralat, M.A., Gregory, J.F. and Hanson, A.D. (2013) A cross-kingdom Nudix enzyme that pre-emptly damage in thiamin metabolism. *Biochem. J.*, **454**, 533–542.
38. Liu, J.Y., Timm, D.E. and Hurley, T.D. (2006) Pyriothiamine as a substrate for thiamine pyrophosphokinase. *J. Biol. Chem.*, **281**, 6601–6607.
39. Mizote, T., Tsuda, M., Smith, D.D.S., Nakayama, H. and Nakazawa, T. (1999) Cloning and characterization of the *thiD/J* gene of *Escherichia coli* encoding a thiamin-synthesizing bifunctional enzyme, hydroxymethylpyrimidine kinase/phosphomethylpyrimidine kinase. *Microbiology*, **145**, 495–501.
40. Toms, A.V., Haas, A.L., Park, J.H., Begley, T.P. and Ealick, S.E. (2005) Structural characterization of the regulatory proteins TenA and TenI from *Bacillus subtilis* and identification of TenA as a thiaminase II. *Biochemistry*, **44**, 2319–2329.
41. Haas, A.L., Laun, N.P. and Begley, T.P. (2005) Thi20, a remarkable enzyme from *Saccharomyces cerevisiae* with dual thiamin biosynthetic and degradation activities. *Bioorg. Chem.*, **33**, 338–344.
42. French, J.B., Begley, T.P. and Ealick, S.E. (2011) Structure of trifunctional THI20 from yeast. *Acta Cryst.*, **D67**, 784–791.
43. Pei, Y., Du, H., Singer, J., Stamour, C., Granitto, S., Shuman, S. and Fisher, R.P. (2006) Cyclin-dependent kinase 9 (Cdk9) of fission yeast is activated by the CDK-activating kinase Csk1, overlaps functionally with the TFIIH-associated kinase Mcs6, and associates with the mRNA cap methyltransferase Pcm1 in vivo. *Mol. Cell. Biol.*, **26**, 777–788.
44. Van Heusden, G.P.H. and Steensma, H.Y. (2006) Yeast 14–3–3 proteins. *Yeast*, **23**, 159–171.
45. Alblova, M., Smidova, A., Docekal, V., Vesely, J., Herman, P., Obsilova, V. and Obsil, T. (2017) Molecular basis of the 14–3–3 protein-dependent activation of yeast neutral trehalase Nth1. *Proc. Natl Acad. Sci. U.S.A.*, **114**, E9811–E9820.
46. Ford, J.C., al-Khodairy, F., Fotou, E., Sheldrick, K.S., Griffiths, D.J. and Carr, A.M. (1994) 14–3–3 protein homologs required for the DNA damage checkpoint in fission yeast. *Science*, **265**, 533–535.
47. Voicu, P.M., Petrescu-Danila, E., Poitelea, M., Watson, A.T. and Rusu, M. (2007) In *Schizosaccharomyces pombe* the 14–3–3 protein Rad24p is involved in negative control of *pho1* gene expression. *Yeast*, **24**, 121–127.
48. Johnstone, T.G., Bazzani, A.A. and Giraldez, A.J. (2016) Upstream ORFs are prevalent translational repressors in vertebrates. *EMBO J.*, **35**, 706–723.
49. Vanoosthuysse, V., Legros, P., van der Sar, S.J., Yvert, G., Toda, K., Le Bihan, T., Watanabe, Y., Hardwick, K. and Bernard, P. (2014) CPF-associated phosphatase activity opposes condensin-mediated chromosome condensation. *PLoS Genet.*, **10**, e1004415.
50. Sanchez, A.M., Garg, A., Shuman, S. and Schwer, B. (2020) Genetic interactions and transcriptomics implicate fission yeast CTD prolyl isomerase Pin1 as an agent of RNA 3' processing and transcription termination that functions via its effects on CTD phosphatase Ssu72. *Nucleic Acids Res.*, **48**, 4811–4826.
51. Ludin, K.M., Hilti, N. and Schweingruber, M.E. (1995) *Schizosaccharomyces pombe rds1*, an adenine-repressible gene regulated by glucose, ammonium, phosphate, carbon dioxide and temperature. *Mol. Gen. Genet.*, **248**, 439–445.
52. Kitamura, K., Katayama, S., Dhut, S., Sato, M., Watanabe, Y., Yamamoto, M. and Toda, T. (2001) Phosphorylation of Mei2 and Ste11 by Pat1 kinase inhibits sexual differentiation via ubiquitin proteolysis and 14–3–3 protein in fission yeast. *Dev. Cell*, **1**, 389–399.
53. Oowatari, Y., Toma, K., Ozo, F. and Kawamukai, M. (2009) Identification of *sam4* as a *rad24* allele in *Schizosaccharomyces pombe*. *Biosci. Biotechnol. Biochem.*, **73**, 1591–1598.
54. Labbé, S., Pelletier, B. and Mercier, A. (2007) Iron homeostasis in the fission yeast *Schizosaccharomyces pombe*. *Biomaterials*, **20**, 523–537.
55. Rustici, G., van Bakel, H., Lackner, D.H., Holstege, F.C., Wijmenga, C., Bähler, J. and Brazma, A. (2007) Global transcriptional responses of fission and budding yeast to changes in copper and iron levels: a comparative study. *Genome Biol.*, **8**, R73.
56. Shah, S., Wittmann, S., Kilchert, C. and Vasiljeva, L. (2014) lncRNA recruits RNAi and the exosome to dynamically regulate *pho1* expression in response to phosphate levels in fission yeast. *Genes Dev.*, **28**, 231–244.
57. Lee, N.N., Chalamcharia, V.R., Reyes-Turce, F., Mehta, S., Zofall, M., Balachandran, V., Dhakshnamoorthy, J., Taneja, N., Yamanaka, S., Zhou, M. et al. (2013) Mtr4-like protein coordinates nuclear RNA processing for heterochromatin assembly and for telomere maintenance. *Cell*, **155**, 1061–1074.
58. Schwer, B., Sanchez, A.M. and Shuman, S. (2020) Inactivation of fission yeast Erh1 de-represses *pho1* expression: evidence that Erh1 is a negative regulator of *pri* lncRNA termination. *RNA*, **26**, 1334–1344.
59. Kilchert, C., Wittmann, S., Passoni, M., Shah, S., Granneman, S. and Vasiljeva, L. (2015) Regulation of mRNA levels by decay-promoting intron that recruit the exosome specificity factor Mmi1. *Cell Rep.*, **13**, 2504–2515.
60. Xie, G., Vo, T.V., Thillainadesan, G., Holla, S., Zhang, B., Jiang, Y., Lv, M., Xu, Z., Wang, C., Balachandran, V. et al. (2019) A conserved dimer interface connects ERH and YTH family proteins to promote gene silencing. *Nature Commun.*, **10**, 251.
61. Vo, T.V., Dhakshnamoorthy, J., Larkin, M., Zofall, M., Thillainadesan, G., Balachandran, V., Holla, S., Wheeler, D. and Grewal, S.I. (2019) CPF recruitment to non-canonical transcription termination sites triggers heterochromatin assembly and gene silencing. *Cell Rep.*, **28**, 267–281.
62. Kelley, L.A., Mezulis, S., Yates, C.M., Wass, M.N. and Sternberg, J.E. (2015) The Phyre2 web portal for protein modeling, prediction and analysis. *Nat. Protoc.*, **10**, 845–858.
63. Ottman, C., Weyand, M., Sassa, T., Inoue, T., Kato, N., Wittinghofer, A. and Oecking, C. (2009) A structural rationale for selective stabilization of anti-tumor interactions of 14–3–3 proteins by cotylenin A. *J. Mol. Biol.*, **386**, 913–919.
64. Jasnovidova, O., Krejčíková, M., Kubicek, K. and Stefl, R. (2017) Structural insight into recognition of phosphorylated threonine-4 of RNA polymerase II C-terminal domain by Rtt103p. *EMBO Rep.*, **18**, 906–913.
65. Kecman, T., Kuš, K., Heo, D.H., Duckett, K., Birot, A., Liberatori, S., Mohammed, S., Geis-Asteggiane, L., Robinson, C.V. and Vasiljeva, L. (2018) Elongation/termination factor exchange mediated by PP1 phosphatase orchestrates transcription termination. *Cell Rep.*, **25**, 259–269.